MEASUREMENTS OF THE THERMAL EXPANSION AND HEAT

CAPACITY OF METALS BY ELECTROMAGNETIC

LEVITATION

Except where reference is made to the work of others, the work described in this thesis is my own or was done in collaboration with my advisory committee.
This thesis does not include proprietary or classified information.

_____

Baojian Guo

Certificate of Approval:

_____	_____
Jeffrey W. Fergus Associate Professor Materials Engineering	Ruel. A. Overfelt, Chair Professor Materials Engineering
_____	_____
Zhongyang Cheng Assistant Professor Materials Engineering	Stephen L. McFarland Acting Dean Graduate School

MEASUREMENTS OF THE THERMAL EXPANSION AND HEAT CAPACITY OF METALS BY ELECTROMAGNETIC LEVITATION

Baojian Guo

A Thesis

Submitted to

the Graduate Faculty of

Auburn University

in Partial Fulfillment of the

Requirements for the

Degree of

Master of Science

Auburn, Alabama
August 7, 2006

MEASUREMENTS OF THE THERMAL EXPANSION AND HEAT

CAPACITY OF METALS BY ELECTROMAGNETIC

LEVITATION

Baojian Guo

Permission is granted to Auburn University to make copies of this thesis at its discretion, upon request of individuals or institutions and at their expense.
The author reserves all publication rights.

_____
Signature of Author

_____
Date of Graduation

VITA

Baojian Guo, son of Liangcai Guo and Feng Xu, was born on January 30, 1977 in Ji'ning, P. R. China. He attended Zhejiang University, Hangzhou, China from September 1996 and obtained a B.S. degree in Mechanical Engineering in 2000. After one year's working for Air Conditioner Division, Midea Co., LTD, Shunde, China, he entered Auburn University pursuing his graduate studies in Materials Engineering in January 2002.

THESIS ABSTRACT

MEASUREMENTS OF THE THERMAL EXPANSION AND HEAT CAPACITY OF METALS BY ELECTROMAGNETIC LEVITATION

Baojian Guo
Master of Science, August 7, 2006
(B.S. in M.E., Zhejiang University, Hongzhou, P.R.China, 2000)

92 Typed Pages

Directed by Ruel A. Overfelt

Electromagnetic levitation is a very useful non-contact melting technique that can be exploited for measurements of thermophysical properties of many reactive metals and alloys. This study focused on thermal expansion and heat capacity measurements based on digital image processing and the modulated power method using the electromagnetic levitation technique (EML). An improved pixel threshold method was developed for accurate determination of the thermal expansion of an axisymmetrically levitated droplet. The modulated power method, originally proposed by Fecht and Johnson (1991), was exploited for measuring the heat capacity of metals in the temperature range of around 1300 to 1800 K. Moffat's uncertainty estimation procedure (Moffat, 1998) was used to theoretically analyze the various contributions to the

experimental uncertainty. A numerical model was developed to examine the sample modulated movement and non-uniform temperature distribution effects during the modulated heating process. The experimental work used different materials including nickel, titanium, zirconium and nickel-based superalloy IN718. The experiments were performed with the electromagnetic levitator of Auburn University.

ACKNOWLEDGMENTS

The author would like to express my grateful appreciation to Dr. Ruel A. Overfelt, whose academic guidance, mentorship, support and patience were invaluable during the entire course of this research. The experience of studying, working with him will have an enormous impact for the career path of the author.

The author would like to thank Dr. Deming Wang for his important suggestions and help throughout the course of this project.

The author also wants to thank my committee members: Dr. Fergus and Dr. Cheng for providing unconditional support and valuable suggestions.

Sincere appreciation is expressed to my research group members, George Teodorescu and Rui Shao, for their support and friendship over the years.

Finally, I would like to thank my wife and my parents and other family members for their love and understanding. It is their constant support, which makes this thesis possible.

Style manual or journal used: Auburn University manuals and guides for the preparation of theses and dissertations

Computer Software used: MS Word 2003, MS Excel 2003 and SigmaPlot 8.0

TABLE OF CONTENTS

LIST OF TABLES xi

LIST OF FIGURES xii

1. INTRODUCTION 1

2. LITERATURE REVIEW 5

2.1. Thermal Expansion Measurement by Image Processing 5

2.2. Specific Heat Measurement by Modulated Power Method 7

3. EXPERIMENT PROCEDURES AND ANALYTICAL TECHNIQUES 10

3.1. Electromagnetic Levitation Apparatus 10

3.2. Sample Image Acquisition and Processing 13

3.3. Modulated Power Method: Control and Data Acquisition 21

3.4. Numerical Model of Modulated Power Method 26

3.4.1. Analysis of Sample Movement due to Modulated Power 26

3.4.2. Analysis of Internal Temperature Field 28

4. RESULTS AND DISCUSSION 32

4.1. Sample Movement Effects 32

4.2. Thermal Expansion of Molten Nickel and Nickel-Based Alloy IN713 34

4.3. Modulated Power Specific Heat Measurements 39

5. CONCLUSIONS 50

6. SUGGESTIONS FOR FUTURE RESEARCH 52

REFERENCES.....53

APPENDICES.....59

A. THE SOURCE CODE FOR THERMAL EXPANSION MEASUREMENT 59

B. THE SOURCE CODE FOR NUMERICAL MODEL OF MODULATED POWER METHOD.....67

C. THE SOURCE CODE FOR ANALYSIS OF TEMPERATURE DATA 76

LIST OF TABLES

Table 3-1. Parameters of Vulcan-I EML coils 22

Table 3-2. Thermophysical properties of liquid nickel samples at the melting temperature of 1728 K 29

Table 4-1. AISI E52100 steel composition (wt %). 34

Table 4-2. Nickel-based superalloy IN713 composition (wt %). 39

Table 4-3. Uncertainty Estimates of the Nickel Specific Heat Measurement using the EML Modulated Power Method. 47

Table 4-4. Uncertainty Estimates of the Titanium Specific Heat Measurement using the EML Modulated Power Method. 48

Table 4-5. Uncertainty Estimates of the Zirconium Specific Heat Measurement using the EML Modulated Power Method. 49

LIST OF FIGURES

Figure 1-1. Schematic sketch of the electromagnetic induction coils with a conducting sample in the middle of the system. 3

Figure 2-1. Radial intensity gradient profile along a levitated droplet. 8

Figure 3-1. Electromagnetic levitator of Auburn University. 11

Figure 3-2. Functional diagram of experimental setup. 12

Figure 3-3. Temperature measurement comparison between pyrometer and thermocouple. 14

Figure 3-4. A levitated spherical solid nickel sample at 1295 ^{o}C. 16

Figure 3-5. Part of the edge of a droplet comparing a fitted sixth order Legendre polynomial with the experimental data..... 19

Figure 3-6. Legendre polynomial of sixth order fit to sample edge coordinates obtained from image processing using the (a) typical gradient method and (b) improved threshold method. 20

Figure 3-7. Vulcan-I EML coil system with a conducting sample in the middle of the system. 22

Figure 3-8. Schematic diagram of modulated heating power method 24

Figure 3-9. Calculated EM force exerted on the levitated sample along axial direction (z-axis). 27

Figure 3-10. (a) Spherical coordinates used in the numerical modeling. (b) Schematic showing the assumed volumetric heating.....30

Figure 4-1. (a) The peak coil current (lower trace) and resultant sample position response (upper trace). (b) Comparison of dynamic temperature response of the sample for motionless and moving sample cases. ω= 0.2 Hz, I_o=122 A, ΔI_o=3 A, I_m=10 A.....33

Figure 4-2. Volume measurements of two steel calibration balls using image processing (a) improved threshold method and (b) maximum intensity gradient method.....36

Figure 4-3. Density of the steel calibration balls.....37

Figure 4-4. Experimentally determined density of electromagnetically levitated liquid nickel samples.....38

Figure 4-5. Experimentally determined density of electromagnetically levitated molten IN713. 41

Figure 4-6. Conductive heat loss through the suspension wire and its effect on heat capacity calculation. 42

Figure 4-7. Heat capacity of nickel: present work and data reported in the literature..44

Figure 4-8. Heat capacity of titanium: present work and data reported in the literature.....45

Figure 4-9. Heat capacity of zirconium: present work and data reported in the literature.....46

1. INTRODUCTION

Information on the temperature dependent thermophysical properties of materials is very important in understanding the complex transport phenomena in materials processes and in obtaining reliable numerical simulations to optimize manufacturing process designs. With the continuous improvements in commercial simulation software, the accuracy of the simulation results is often limited by the accuracy of the input materials properties. However, such data can be extremely difficult to measure if high temperatures are involved and the material exhibits significant chemical reactivity with crucibles.

Electromagnetic levitation (EML) technology has been applied to containerless processing of liquid metals from the 1930s with benefits in both process control and product quality. Electrically conductive metals can be levitated by magnetic fields under clean environmental conditions. The eddy currents provide an effective means for stirring. These effects can significantly improve uniformity of compositions and mechanical properties. During solidification, heterogeneous nucleation on the container wall is eliminated.

EML technology has recently attracted interest for thermophysical property measurements to alleviate deleterious crucible containment affects in earth-based laboratories as well as in space. For example, EML has been utilized in a recent series of orbital experiments with the TEMPUS electromagnetic levitator (Egry et al., 2001;

Wunderlich et al., 2001).

Most electromagnetic levitation coils consist of two sets of opposing turns: the top coil and the bottom coil. The top coil and bottom coil are wound in different directions. When a conductive sample is placed inside of the electromagnetic induction coils that are carrying high frequency alternating current, eddy currents are induced in the sample. The bottom set of coils always provide the lifting force to oppose gravity due to the mutually repulsive interaction between the fields around the coils and the sample's induced field. Since the mutual repulsive nature between the induced field and externally applied electromagnetic field, the sample moves towards the weakest part of the applied field. The top set of coils provides stability in the lateral direction. A schematic of the applied electromagnetic fields inside the electromagnetic levitation coils is shown in Figure 1-1.

Electromagnetic levitation experiments can also be performed in micro-gravity. Space-based electromagnetic levitators (e.g., TEMPUS), designed to operate under micro-gravity, use two sets of independent coaxial induction coils. The small positioning forces necessary in low-g are provided by one coil while the heating power is provided by an additional higher frequency coil. The sample's temperature can thus be controlled over a wide range depending upon the specific sample size and properties.

Earth-based electromagnetic levitation systems typically use only a single set of opposing coils of the quadrapole design and operated at a single frequency to both levitate and heat the sample. Although the heating and levitation effects are coupled, such systems are easy to fabricate, assemble and operate. An example of such a single coil system is the Vulcan-I instrument originally developed for operation in the earth-based laboratory as well as on parabolic flights of NASA's KC135 low-g research aircraft

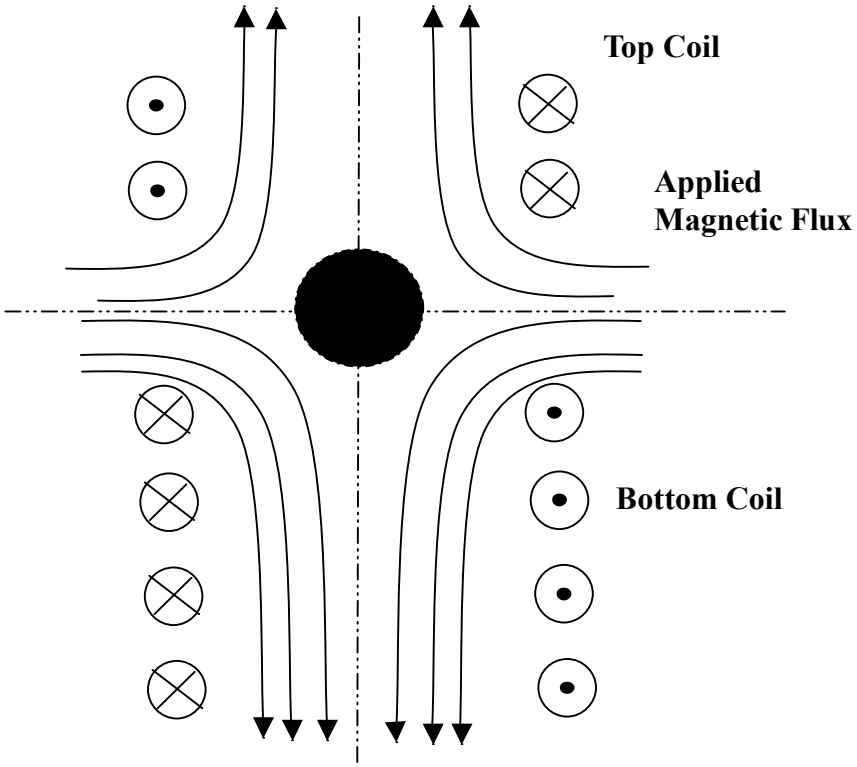

Figure 1-1. Schematic sketch of the electromagnetic induction coils with a conducting sample in the middle of the system.

(Chen and Overfelt, 1998; Wang et al., 2003).

A very promising feature of EML is its potential for measuring several important thermophysical properties on a single levitated sample over a large temperature range. The absence of crucibles eliminates reactions with the melt and high levels of undercooling can also be reached. Such applications require sophisticated non-contact diagnostics such as two-color pyrometry for temperature measurement and high-speed video analysis for characterizing the sample motion. The thermophysical properties of typical interest are surface tension, density and thermal expansion, emissivity, specific and latent heats, thermal conductivity and electrical conductivity. Reviews of theoretical and experimental work in this area are given by Herlach et al. (1993) , Egry et al.(1993) and Bakhtiyarov and Overfelt (2002; 2003).

More recently, high-temperature electrostatic levitation (HTESL) has been developed at NASA's Jet Propulsion Laboratory (Chung et al., 1996) . HTESL charges a sample and then uses electrostatic repulsive forces to levitate and position the charged sample. A separate optical power system (laser, focused lamp, etc.) is needed to heat the sample. HTESL systems are inherently unstable and require complex monitoring and control systems for reliable operation. Nevertheless, HTESL can be applied to electrical non-conducting materials as well as conductive materials.

This study intended to develop a new digital image processing method to accurately measure the thermal expansion of levitated solid and molten metals and to implement the modulated power method of specific heat measurement on different sizes of solid samples. In addition, a numerical model was developed to examine the heat transfer phenomena and examine the uncertainty in the heat capacity measurements.

2. LITERATURE REVIEW

2.1. Thermal Expansion Measurement by Image Processing

Thermal expansion is an important thermophysical property in materials science. Since direct physical contact is avoided in EML, standard push rod dilatometry cannot be applied for measurements of thermal expansion. Sample images taken with precise optical systems are required to characterize the sample sizes and evaluate thermal expansion effects. When a sample is levitated and heated by an induction coil, the volumes of symmetrical samples can be determined from side view images. However careful coil design and fabrication is required to establish stable heating and levitation conditions necessary for symmetrical molten droplets in typical earth-based EML laboratories.

In previous work (El-Mehairy and Ward, 1963), electromagnetically levitated samples were photographed from the side using high speed film cameras. A photographic enlarger was then used to achieve the necessary resolution for density measurements. The edges of the samples for each image were determined by hand, and the volumes were then obtained as a body of revolution from the edge profiles. This is a very inefficient method and also inevitably involved random errors caused by each individual experimenter. The modern development of CCD (charged-couple device) cameras and digital image processing technique enable electromagnetically levitated sample images to be automatically recorded and the recorded images analyzed using digital image processing

technique.

The key issue of accurate volume measurement is precise and repeatable detection of the droplet edge in the images. An edge is defined as the boundary between two regions with relatively distinct gray-level properties. Most edge detection algorithms are based on the computation of a local gradient operator where the edge is at the location of the maximum intensity gradient. Because of the intrinsic sensitivity of taking derivatives from experimental data, the gradient method is very sensitive to noise and has demanding requirements for picture quality (Gonzalez and Wintz, 1987; Jain, 1989). Several researchers in electromagnetic levitation have adopted first-order derivative gradient operators to determine the sample edge from image data (Brillo and Egry, 2003; Chung et al., 1996; Damaschke et al., 1998; Gorges et al., 1996; Racz and Egry, 1995).These techniques detected the edge by searching for the maximum intensity gradient along radial vectors of each picture. Second-order derivative operators have also been reported (Racz and Egry, 1995). Figure 2-1 shows a typical intensity gradient profile along a levitated sample radial direction. Figure 2-1 (a) is the intensity first-order derivative profile and figure 2-1 (b) is the intensity second-order derivative profile. However, as noted above, gradient methods have strict requirements on picture quality and thus backlighting techniques have been adopted to reduce pixel blooming in CCDs and improve contrast (Brillo and Egry, 2003; Chung et al., 1996; Damaschke et al., 1998). Pixel blooming occurs when a pixel's electrical charge exceeds the CCD pixel's storage limit and then the electrical charge overflows to neighboring pixels.

A robust alternative approach to analysis of noisy images involves threshold methods (Gonzalez and Wintz, 1987; Jain, 1989). Racz and Egry (1995) and Gorges et al

(1996) noticed that hotter and brighter samples exhibited less image contrast than cooler samples when the images were due to emitted radiation. These researchers adopted a pixel threshold image processing method but still experienced considerable scatter in their measured sample volumes. The present research introduces the use of the image of the water cooled electromagnetic coil (of known diameter) to determine the specific pixel threshold value for edge detection for each individual image. This approach enables precise and accurate determination of levitated sample edges without the need for sample backlighting.

2.2. Specific Heat Measurement by Modulated Power Method

Accurate knowledge of heat capacity of materials is very important for both fundamental studies on phase transformations and optimization of industrial processes. Experimental measurements of heat capacity can also be used to derive enthalpy, entropy and the Gibbs free energy -- essential thermodynamic parameters.

Although differential scanning calorimetry (DSC) is a very fast, accurate, and convenient method for numerous applications, serious contamination can occur between the sample and crucible when the measurement is carried out at high temperature. Non-contact techniques such as electromagnetic levitation (EML) must be applied when sample – crucible interactions may corrupt the experimental data.

Ohsaka and Schaefers (1992; 1995) successfully coupled the EML technique with a drop calorimeter and measured the specific heat of elemental nickel, iron, vanadium, and niobium. The enthalpy of each sample was indirectly measured by the temperature increase of the calorimeter after dropping the levitated hot sample into the calorimeter. This approach overcame the sample – container contamination associated

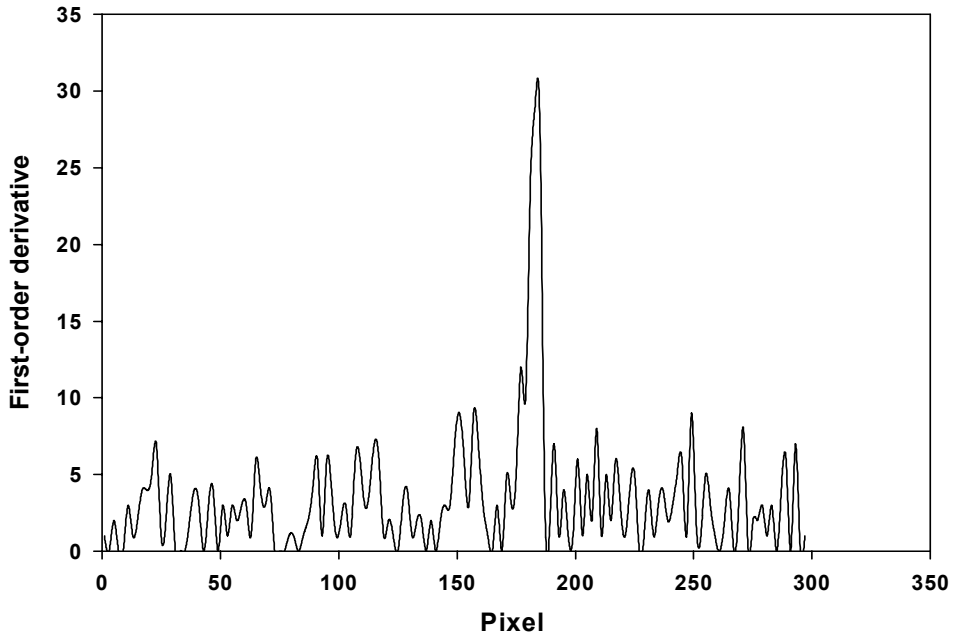

(a)

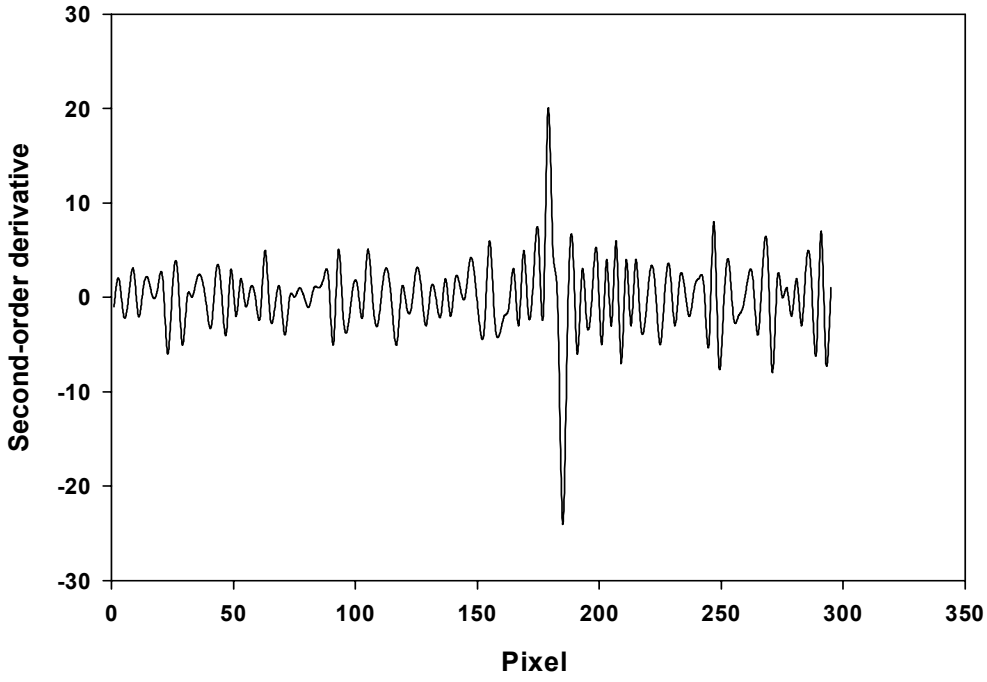

(b)

Figure 2-1. Radial intensity gradient profile along a levitated droplet.

(a) First-order derivative profile. (b) Second-order derivative profile.

with conventional calorimeters. However, it introduced significant experimental complexity and only allowed a single point measurement of enthalpy with each sample processed. In the pioneering modulated power experiments (Bachmann et al., 1972; Sullivan and Seidel, 1968), heat capacity measurement was performed at low temperatures with a small sample (1-500mg) and in which a silicon chip was used as the sample holder. Fecht and Johnson (1991) and their colleagues (Fecht and Wunderlich, 1994; Wunderlich et al., 1993; Wunderlich et al., 2000; Wunderlich et al., 2001; Wunderlich and Fecht, 1993; Wunderlich and Fecht, 1996; Wunderlich et al., 1997) applied the modulated power method to the electromagnetic heating and levitation technique. In this application, the electromagnetically heated and levitated sample is exposed to a slowly varying sinusoidally-modulated heating power. The temperature response of the levitated sample slightly lagged behind the imposed power profile with a time constant that depended upon the thermal inertia of the sample. By proper choice of the modulation frequency, the transient effects of external and internal thermal relaxations can be ignored with errors of only approximately 1% (Fecht and Johnson, 1991). The unknown specific heat can then be calculated if the sample's emissive properties are known. The electromagnetic levitation technique (Egry et al., 1993; Wroughton et al., 1952) combined with the modulation power method is an excellent experimental technique that allows containerless heat capacity measurements on electrically conductive samples.

3. EXPERIMENT PROCEDURES AND ANALYTICAL TECHNIQUES

3.1. Electromagnetic Levitation Apparatus

A key part of the electromagnetic levitator at Auburn University (Figure 3-1.) is the induction coil housed in a vacuum chamber (10^{-6} torr) pumped by a turbomolecular pump. A sample handler with a rotational sample selector allows up to 8 samples to be processed without opening the vacuum chamber. A commercial 1 kW RF power supply is used to provide a high frequency alternating current of approximately 175 amps at 280 kHz to the induction coil. The induction coil was configured to impose a quadrupole positioning field to keep the sample approximately in the middle of the coil. One of the advantages of the quadrapole design is that the system is very simple, easy to make with high degree of symmetry and exhibits a stably levitated sample.

The RF power supply is controlled by a computer and D/A converter using RS232 Serial Interfaces. The power supply control signal is composed of a DC component and an AC component. A functional diagram of the experimental setup is shown in figure 3-2.

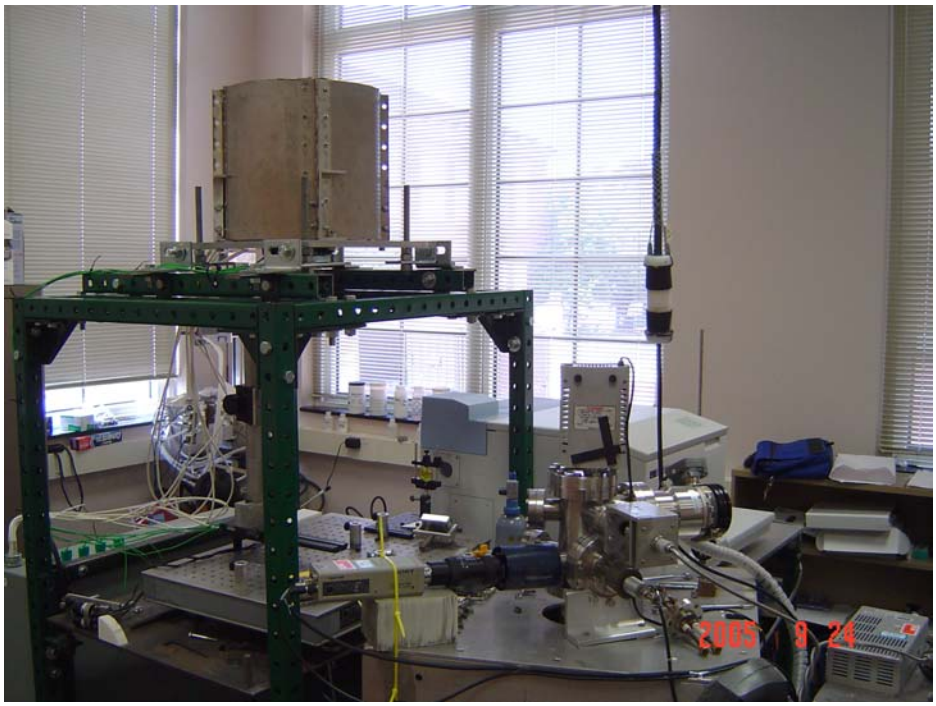

Figure 3-1. Electromagnetic levitator of Auburn University.

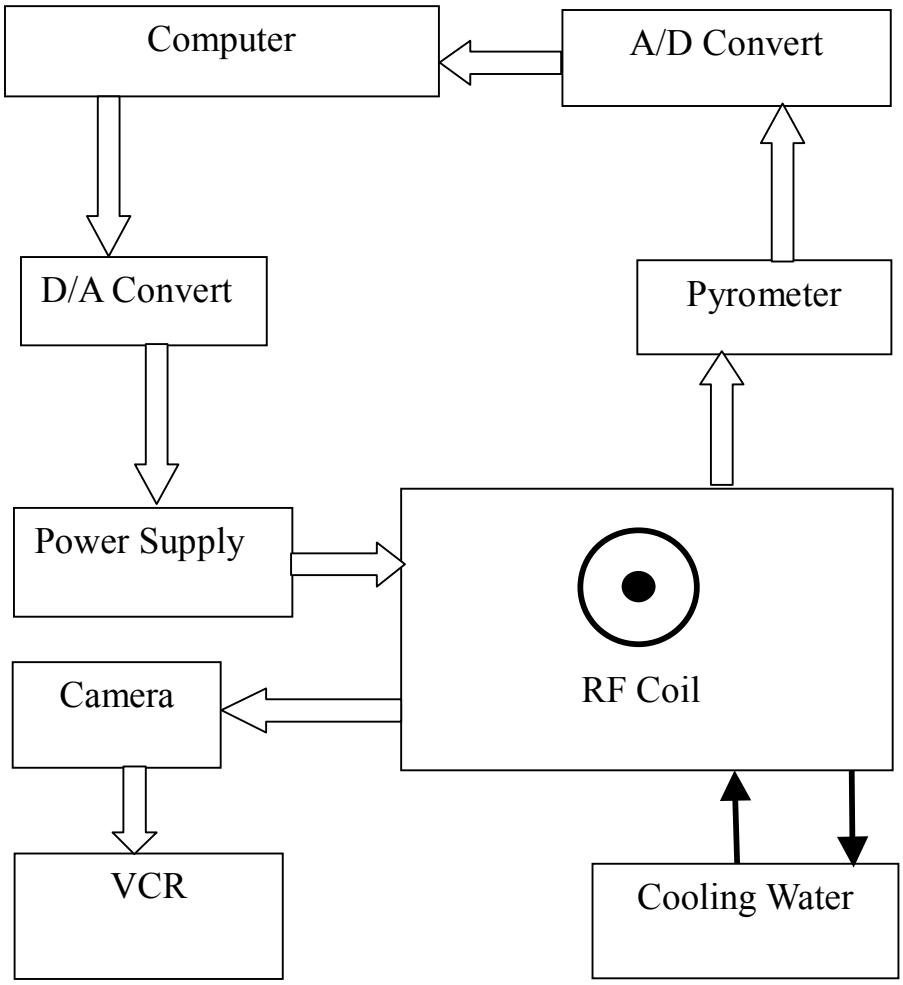

Figure 3-2. Functional diagram of experimental setup.

A Micron 2-color pyrometer with 0.5% reported uncertainty was used to characterize the thermal response of all samples. A solid cylindrical zirconium sample with 6 mm diameter and 6.2 mm height was suspended by 0.15 mm diameter R-type thermocouple wire attached to the sample. Four separate transient heating experiments from room temperature to1423 K, 1498 K, 1673 K and 1773 K were conducted in the induction coil. The results (See Figure 3-3) indicated that the temperature measurements between the pyrometer and the thermocouple agreed to within 0.4% during steady state measurements and approximately 0.8% during the transient heating conditions. In addition, the pyrometer's calibration was checked by a comparison with samples of pure nickel at the melting temperature of 1728 K, the pyrometer showed a slightly smaller measurement, the agreement with the reference melting temperature was 0.52%.

3.2. Sample Image Acquisition and Processing

A CCD camera is used to monitor the experiment and record sample image data from the side. Under normal conditions, the sample is at a high enough temperature that the emitted radiation is sufficient for direct illumination on the photodetector. All images for thermal expansion measurements were taken with a Watec LCL-903HS CCD camera (resolution of 768 X 494) at 30 frames per second and a shutter speed of 1/1000 second.

The central challenge of the image processing is to separate the droplet from the background. The droplet edge is located at the transition region of the intensity profile. In the threshold method, if the intensity of a certain pixel is higher than a threshold value, the pixel is considered in the region of the droplet. If the intensity of a certain pixel is less than a threshold value, the pixel is considered in the background. The key issue is how to determine the threshold intensity value for each image. The water-cooled coil tubing (of

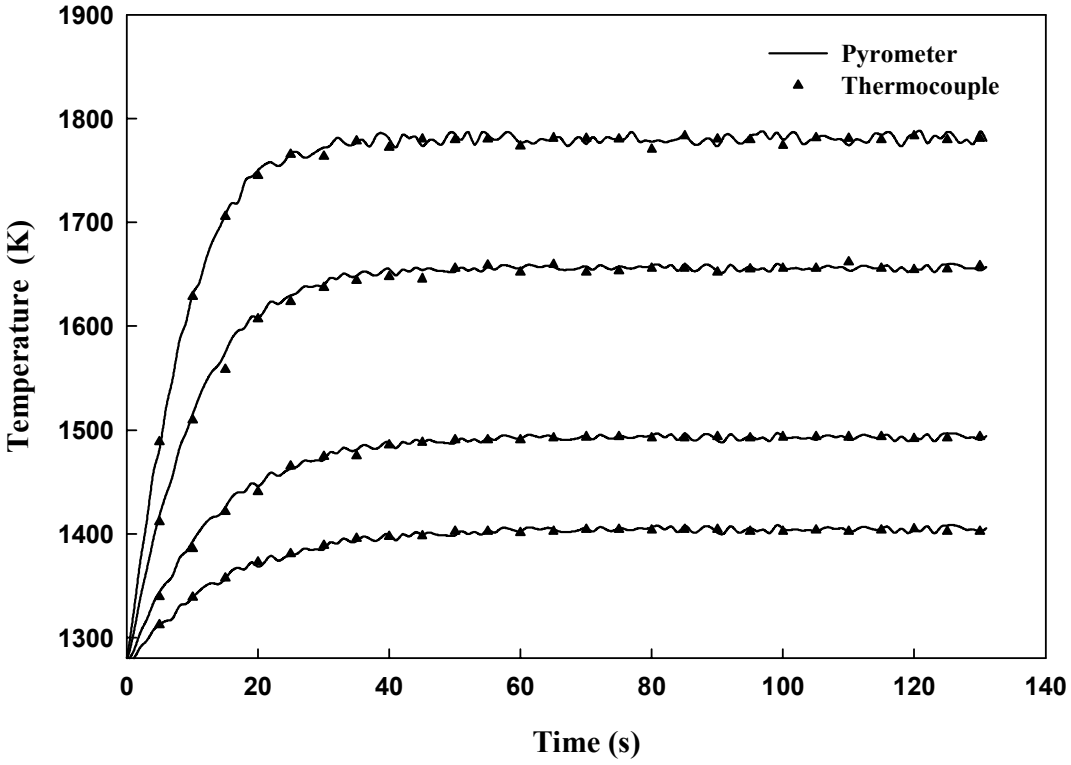

Figure 3-3. Temperature measurement comparison between pyrometer and thermocouple.

known diameter in each image) in the present experiments provides a convenient reference to determine (1) the optical system magnification and (2) the unique pixel threshold value for each image. See Figure 3-4.

The optical system magnification is easily determined using vertical scans across the coil tube on images with samples at low temperatures. Typically 30-40 images are processed using the maximum intensity gradient method to evaluate the number of pixels that represent the tubing diameter. The gradient technique works well with samples at low temperatures since blooming effects are negligible. Then the threshold pixel intensity value representing the edge of the coil tubing is characterized for every image since the number of pixels for the tubing diameter will not change. This process determines for each particular image, regardless of the sample brightness, the unique threshold pixel value for a bright sample and dark background/foreground.

When the threshold transition value of the edge between the bright sample pixels and the dark coil pixels is obtained, the center of the sample is identified as follows. A matrix of ten horizontal lines and ten vertical lines are scanned across the sample image and the sample edges identified using the threshold pixel transition value as evaluated above. The center of the sample is then estimated as the average of the ten values with $X_0 = (X_{edge,max} - X_{edge,min})/2$ and $Y_0 = (Y_{edge,max} - Y_{edge,min})/2$. After the sample center is identified, a set of 360 equally spaced radial vectors (one degree per vector) is established from the sample center outward and the sample edge locations determined using the threshold pixel transition value to distinguish the bright sample from the dark background.

The edge point data are then fit with a sixth order Legendre polynomial. Eq.(1) describes the curve fitting function:

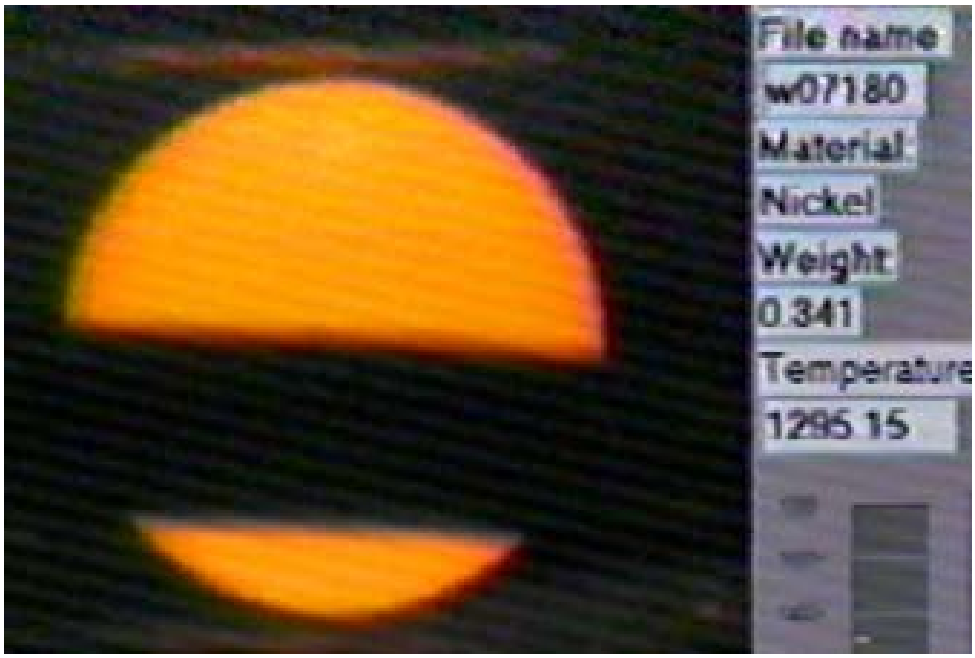

Figure 3-4. A levitated spherical solid nickel sample at 1295 ^{o}C.

Note the “horizontal” coil blocking part of the image.

$$R_{fit}(\theta) = \sum_{j=0}^{6} a_j P_j(\cos(\theta)) \quad (1)$$

where $P_j(\cos(\theta))$ are the Legendre polynomials and a_j are the polynomial coefficients. The curve fitting is implemented with a standard least-squares procedure. The curve fitting procedure provides a complete definition of the sample's edge even though the coil blocks part of the sample image. In addition, the curve fitting procedure actually improves upon the one-pixel resolution of the image.

Since surface tension ensures a molten sample's surface remains relatively smooth, large deviations in a droplet's edge data are not physically possible. A typical set of edge data and the fitted polynomial are shown in figure 3-5. The data point marked by the arrow is clearly an outlier and should not be used in the edge determination procedure. The fitting residuals between the locations of the experimental data points and the fitted curve are examined and all edge points with a residual greater than 2σ are discounted and eliminated from the experimental data set. After the outliers are removed, the data are then fit again with a new sixth order Legendre polynomial.

Figure 3-6 shows a comparison of curve fits after the droplet edge data were determined by the typical maximum intensity gradient method and the improved threshold method as outlined above. The improved threshold method provides much better agreement with the experimental data. The improved threshold method was also found to be a more accurate approach, as will be discussed later in the experiment results section.

Assuming that the sample is axisymetric, the droplet volume can then be calculated as a body of revolution from the smooth curve as

$$V = \frac{2\pi}{3}\int_0^{\pi} R(\theta)^3 \, Sin(\theta) d\theta \qquad (2)$$

Once the volume is determined, the density is easily calculated if the sample mass is known. In the present experiments, the mass of the each sample was carefully evaluated before and after the experiment and evaporation was assumed to occur linearly with time while the sample was molten. The value of dV/dT for molten metals is of the order of 10^{-4} $g\ cm^{-3}\ K^{-1}$. The error analysis of Racz and Egry (Racz and Egry, 1995) show that edge location using pixel interpolation combined with Legendre polynomial fitting enable theoretical volume uncertainties of $\Delta V/V \sim 10^{-4}$.

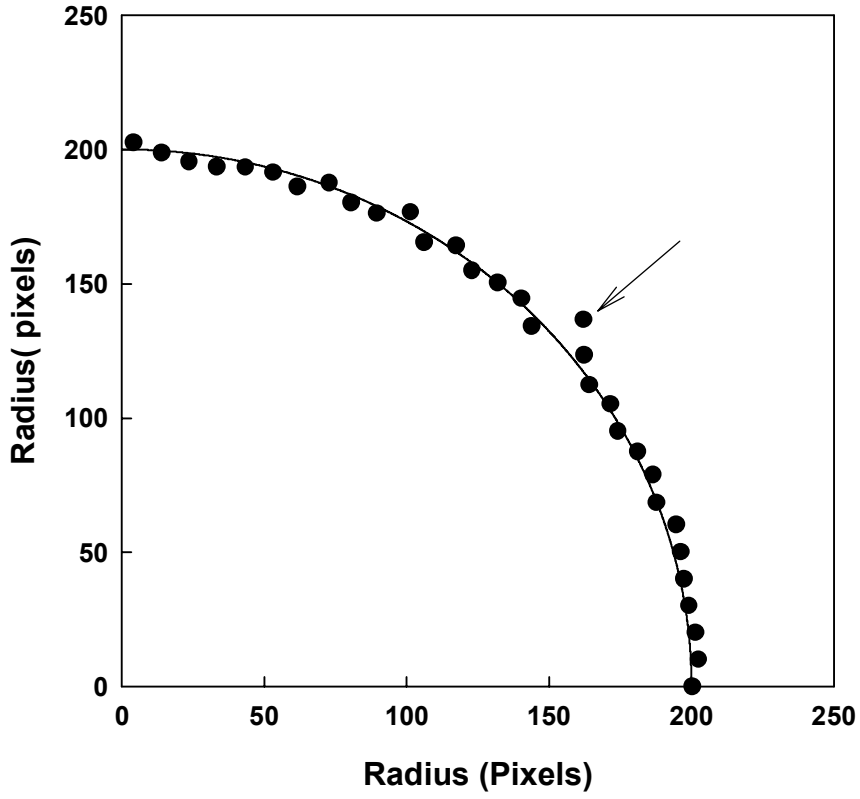

Figure 3-5. Part of the edge of a droplet comparing a fitted sixth order Legendre polynomial with the experimental data. A clearly erroneous experimental data point is identified.

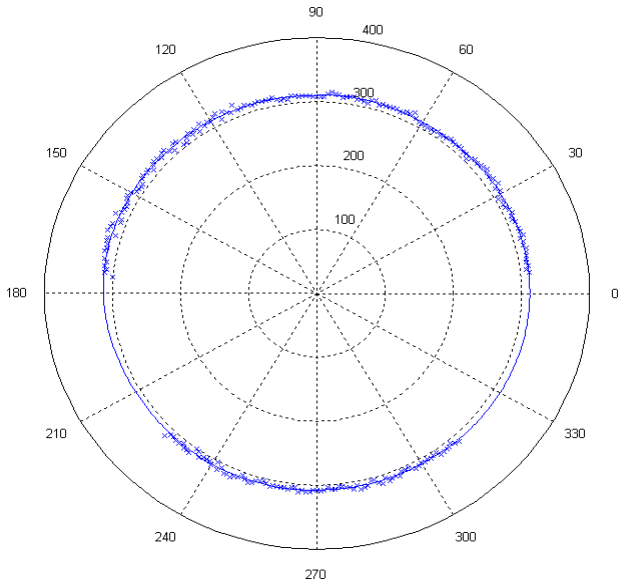

(a)

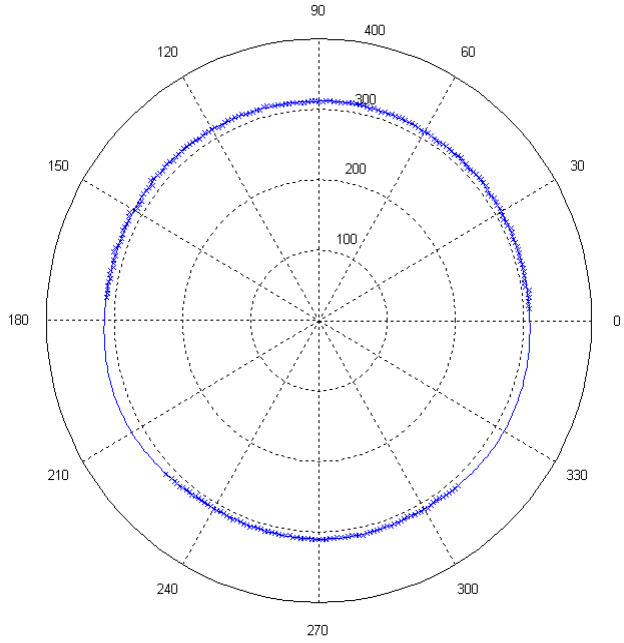

(b)

Figure 3-6. Legendre polynomial of sixth order fit to sample edge coordinates, obtained from image processing using the (a) typical gradient method and (b) improved threshold method.

3.3. Modulated Power Method: Control and Data Acquisition

Okress et al.(1952), Fromm and Jehn (1965) and Xuan (2000) assumed that the sample is much smaller than the size of the induction coils and treated the levitated sample as a circular current loop. Xuan derived the time-averaged axial (i.e., *z*) levitation force *F(z)* and power absorption *P(z)* expressions, for Vulcan-I RF coil system in figure 3-7, as:

$$F(z) = \frac{9}{8}\mu I_{peak}^2 G(x) S_n \tag{3}$$

and

$$P(z) = \frac{3}{4} R\pi\sigma^{-1} I_{peak}^2 F(x) H(z) \tag{4}$$

where

$$G(x) = 1 - \frac{3\sinh(2x) - 3\sin((2x)}{4x\sinh^2(x) + 4x\sin^2(x)} \tag{5}$$

$$S_n = \sum_n \frac{b_n^2}{[b_n^2 + (z - z_n)^2]^{1.5}} \sum_n \frac{b_n^2 (z - z_n)}{[b_n^2 + (z - z_n)^2]^{2.5}} \tag{6}$$

$$F(x) = \frac{x\sinh(2x) + x\sin(2x) - \cosh(2x) + \cos(2x)}{\cosh(2x) - \cos(2x)} \tag{7}$$

$$H(z) = \{\sum_n \frac{b_n^2}{[b_n^2 + (z - z_n)^2]^{1.5}}\}^2 \tag{8}$$

and $$x = R\sqrt{\pi\mu f\sigma} \tag{9}$$

Here, μ is magnetic permeability of the sample, R is sample's radius, σ is the sample's electrical conductivity, I_{peak} is the maximum current of the induction coil, and f is the current frequency. The geometric configuration for the coil set is summarized in Table 3-1.

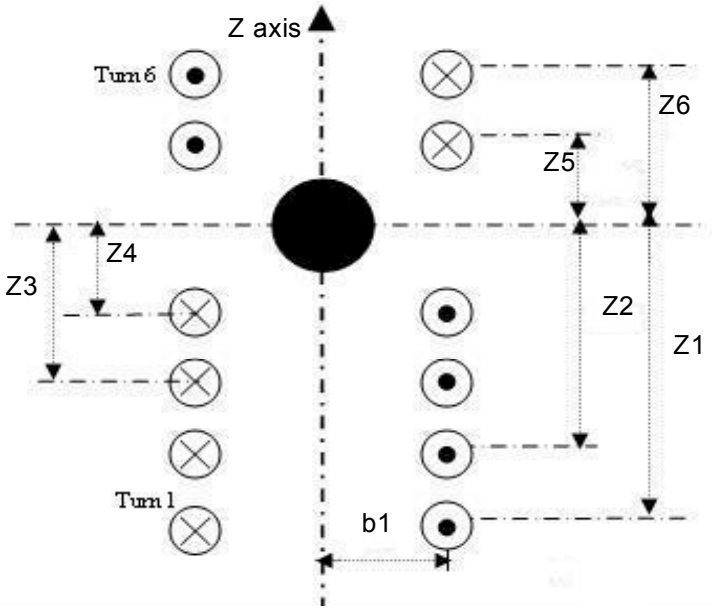

Figure 3-7. Vulcan-I EML coil system with a conducting sample in the middle of the system.

Table 3-1. Parameters of Vulcan-I EML coils.

Coil Set radius(mm)x turns	Z1 (mm)	Z2 (mm)	Z3 (mm)	Z4 (mm)	Z5 (mm)	Z6 (mm)
4.5 x 6	-8.44	-6.24	-4.04	-1.84	1.84	4.04

(Origin is located at the middle of the gap between upper coils and lower coils)

Figure 3-8 shows a typical thermal response for the model system. In this application of the modulation power technique, a spherical sample is heated by a total power which can be expressed as:

$$P_{total} = P_o + \Delta P_o + \Delta P_\omega \cos(\omega t) \tag{10}$$

where P_o is the steady power, ΔP_ω is the modulation component of power and ΔP_o is the net increase in steady power due to the modulation. The sample's temperature response also exhibits three components: the bias temperature T_o, related to P_o, an oscillatory component ΔT_ω induced by ΔP_ω, and a net increase in bias temperature ΔT_o due to ΔP_o. Theoretically, the amplitude of ΔT_ω is given by (Bachmann et al., 1972; Fecht and Johnson, 1991; Sullivan and Seidel, 1968):

$$\Delta T_\omega = \frac{\Delta P_\omega}{\omega \rho V C_p} [1 + (\omega \tau_1)^{-2} + (\omega \tau_2)^2]^{-1/2} \tag{11}$$

Here τ_1 is the sample's external relaxation time and τ_2 is the sample's internal relaxation time, defined as:

$$\tau_1 = \frac{\rho V C_p}{4 A \varepsilon \sigma_{SB} T_o^3} \tag{12}$$

$$\tau_2 = \frac{3 \rho V C_p}{4 \pi^3 \kappa R} \tag{13}$$

κ is sample's thermal conductivity, ρ is sample's density, V is the sample volume, A is the sample surface area and σ_{SB} is Stefan's constant. As noted by Fecht and Johnson (1991), if the modulation frequency is appropriately chosen (~0.1 – 0.5 Hz for typical metal samples in earth-based levitation systems), the transient effects of external and internal thermal relaxations can be ignored with errors of only approximately 1%.

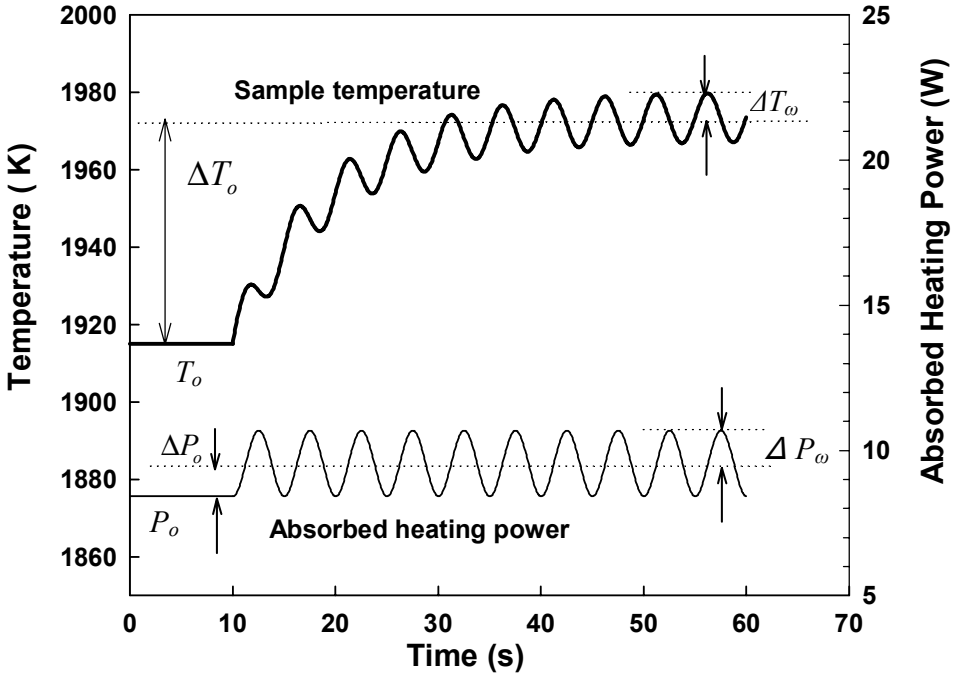

Figure 3-8. Schematic diagram of modulated heating power method

Thus Eq.(11) reduces to:

$$\Delta T_{\omega} = \frac{\Delta P_{\omega}}{\omega \rho V C_p} \tag{14}$$

A control voltage is applied to the power supply of the RF system, and the current in the electromagnetic coil can be represented as:

$$I_{peak}(t) = I_o + I_m \cos(\omega t) \tag{15}$$

Substituting Eq.(15) in Eq.(4), the total power can be formulated as:

$$P_{total} = P_o + \Delta P_o + \Delta P_{\omega} \cos(\omega t) + \Delta P_{2\omega} \cos(2\omega t) \tag{16}$$

where,

$$P_o = \frac{3}{4} R \pi \sigma^{-1} I_o^2 F(x) H(z) \tag{17}$$

$$\Delta P_o = \frac{3}{8} R \pi \sigma^{-1} I_m^2 F(x) H(z) \tag{18}$$

$$\Delta P_{\omega} = \frac{3}{2} R \pi \sigma^{-1} I_o I_m F(x) H(z) \tag{19}$$

and

$$\Delta P_{2\omega} = \Delta P_o \tag{20}$$

At steady state in vacuum, the input power P_o is just balanced by the radiative heat losses. When the coil current is modulated, the bulk sample temperature will rise by ΔT_o due to the increase ΔP_o in average absorbed power as shown in figure 3-8. Although the temperature signal should theoretically contain a 2ω frequency component, this component is <1% due to $I_m << I_o$. Determination of the specific heat from Eq. (14) requires knowledge of the power modulation amplitude ΔP_{ω} from the sample's temperature response. For a motionless sample, ΔP_{ω} can be estimated from P_o as:

$$\Delta P_{\omega} = \frac{2 I_m}{I_o} P_o \tag{21}$$

where P_o is experimentally obtained using the Stefan-Boltzmann law:

$$P_o = A\sigma_{SB}\varepsilon[T_o^4 - T_{env}^4] \tag{22}$$

in which T_{env} is surrounding environment temperature.

3.4. Numerical Model of Modulated Power Method

3.4.1. Analysis of Sample Movement due to Modulated Power

In the presence of modulation current in the form of Eq.(15), the total levitation force can be expressed by Eq.(23) when neglecting the 2ω frequency component.

$$F_{total} = F_o + \Delta F_o + \Delta F_\omega \cos(\omega t) \tag{23}$$

where:

$$F_o = \frac{9}{8}\mu I_o^2 G(x) S_n \tag{24}$$

$$\Delta F_o = \frac{9}{16}\mu I_m^2 G(x) S_n \tag{25}$$

$$\Delta F_\omega = \frac{9}{4}\mu I_o I_m G(x) S_n \tag{26}$$

With knowledge of the time-averaged levitation force and modulated current form, mathematical expressions can be quickly developed for analyzing the sample's oscillatory motion. Figure 3-9 shows a typical theoretical levitation profile on a nickel sample in the coil design used in the current experiments. The equilibrium levitation position is indicated by the arrow. When the sample deviates from its equilibrium position, a restoring force proportional to the displacement is exerted on the sample. Therefore, a simple spring mass system can be used to describe the oscillatory motion of levitated samples.

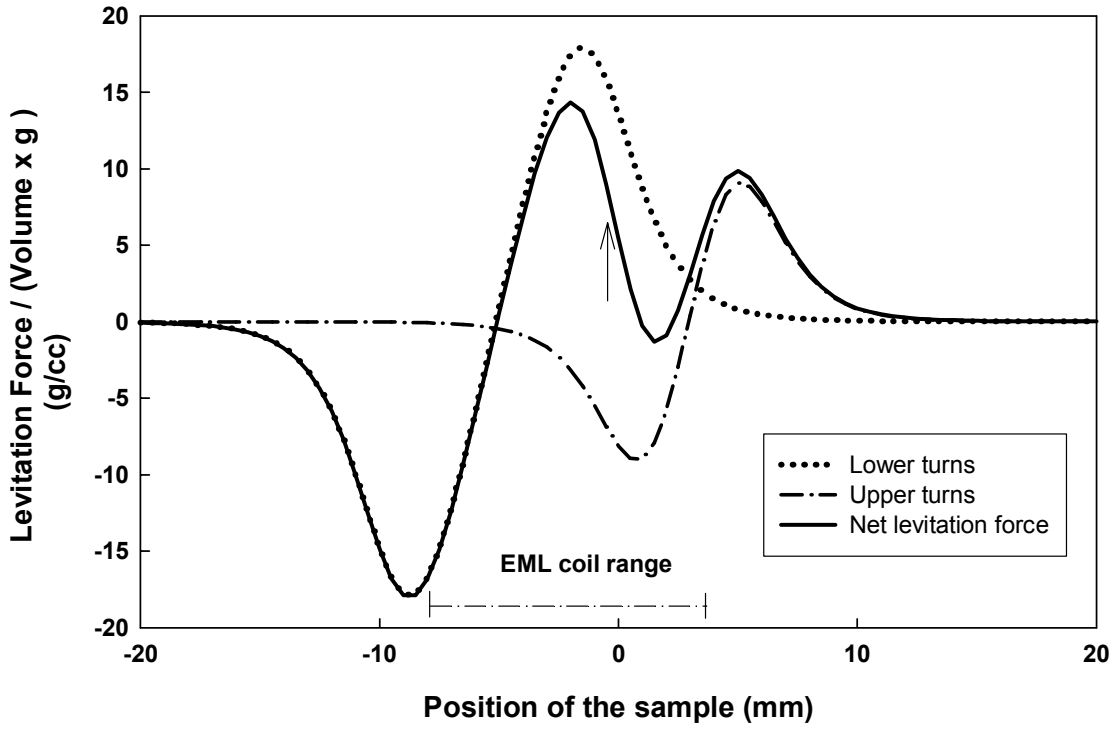

Figure 3-9. Calculated EM force exerted on the levitated sample along axial direction (z-axis). Coil Current (peak): 130A, Frequency: 200 KHz. The equilibrium position corresponding to the sample density is indicated

F_o is the steady levitation force in the absence of any power modulation. ΔF_o is the increased bias of the steady levitation force due to the modulation effects. Thus the equilibrium position is increased slightly due to the power modulation. ΔF_ω is the amplitude of the modulation force term, which will cause the oscillatory motion. Assuming that ΔF_o and ΔF_ω are constant and calculating S_n at the new sample equilibrium position enables the modulation movement to be fully described by a spring-mass system with an external oscillatory driving force. The sample will vibrate in forced harmonic motion around its new equilibrium position at the driving frequency ω. The motion of the sample is governed by Newton's second law:

$$m\frac{d^2z}{dt^2} + kz = \Delta F_\omega \cos(\omega t) \tag{27}$$

where m is the sample mass and k is the spring constant determined from the levitation force profile. The natural frequency of typical metal samples in typical levitation systems is about 10 Hz. As noted earlier, the modulation frequencies for heat capacity measurements are typically 0.1-0.5 Hz, fortunately well below the natural frequency of the levitation system.

3.4.2. Analysis of Internal Temperature Field

A simplified heat transfer model was developed considering internal conduction and external radiation for spherical solid samples undergoing uniform induction heating around an equatorial band extending ±10° (north and south) from the equator. The governing heat transfer equation in spherical coordinates (Figure 3-10 (a)) is given by:

$$\rho V C_p \frac{\delta T}{\delta t} = k\left[\frac{\delta}{r^2 \delta r}\left(r^2 \frac{\delta T}{\delta r}\right) + \frac{\delta}{r^2(\sin\theta)\delta\theta}\left(\sin\theta \frac{\delta T}{\delta\theta}\right) + \frac{1}{r^2 \sin^2\theta}\left(\frac{\delta^2 T}{\delta^2 \varphi}\right)\right] + \dot{Q} \tag{28}$$

where the heat generation term $\dot{Q}$ only existed in the inductively heated region. The penetration depth of induction heating is given by:

$$\delta = \sqrt{\frac{2}{\omega \sigma \mu_0}} \tag{29}$$

Figure 3-10 (b) is the schematic showing the simplified heating assumed. Table 3-2 lists the thermophysical properties of liquid nickel used for the heat transfer analysis. The sample size investigated was 4 mm diameter.

Table 3-2. Thermophysical properties of liquid nickel samples at the melting temperature of 1728 K (Brandes and Brook, 1992) .

Parameters	Value	Unit
density *(ρ)*	7.905	g cm^{-3}
emissivity *(ε)*	0.22	
specific heat *(C_p)*	620	J $kg^{-1}k^{-1}$
thermal conductivity *(k)*	76	$wm^{-1}k^{-1}$
electrical conductivity *(σ)*	$5 \cdot 10^6$	$(\Omega m)^{-1}$
saturated pressure *(P_s)*	0.0029	torr

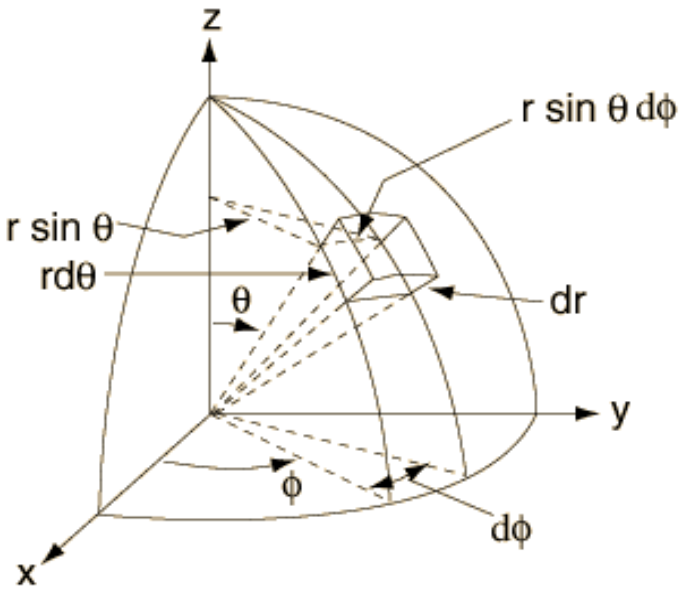

(a)

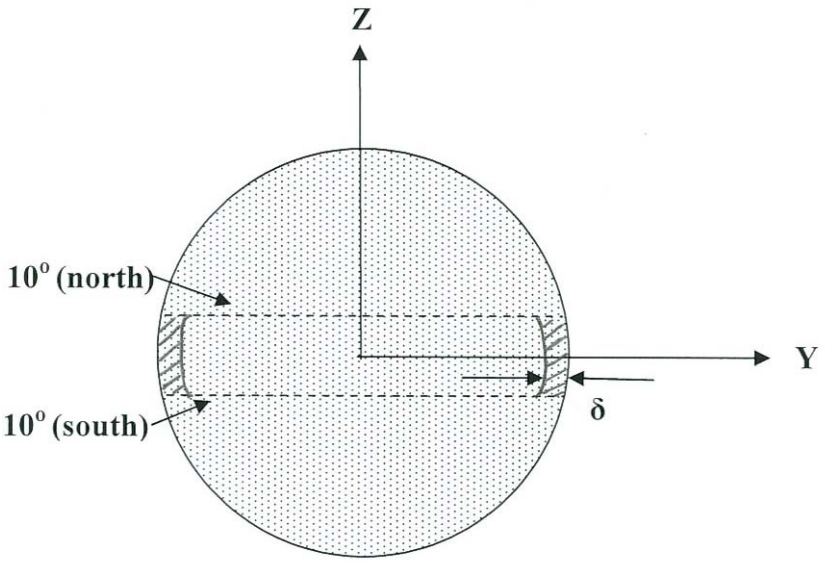

(b)

Figure 3-10. (a) Spherical coordinates used in the numerical modeling.

(b) Schematic showing the assumed volumetric heating.

The electromagnetic heating power was assumed to be uniformly distributed in a shell volume region defined by the sample surface (latitudes from 10° north to 10° south) and the penetration depth. Electromagnetic levitation systems typically operate at 100-500 kHz. Thus for this analysis of the modulated power method using frequencies of 0.1-0.5 Hz, the induced heating currents can be assumed to instantaneously rise to their peak values. The radiation heat losses were linearized as:

$$q_{rad} = h_{ra} A (T_{l+1} - T_{env}) \tag{30}$$

with

$$h_{ra} = \sigma_{SB} \varepsilon (T_l^2 + T_{env}^2)(T_l + T_{env}) \tag{31}$$

where, the subscripts l, and l+1 denote the times t and $t+\Delta t$.

4. RESULTS AND DISCUSSION

4.1. Sample Movement Effects

The dynamic response of a levitated 4 mm diameter nickel sample in the modulated heating process was theoretically calculated as described in Section 3.4.1. A typical example of representative result for normal levitation conditions is shown in figure 4-1.(a). The lower trace of figure 4-1.(a) shows the induction coil peak current calculated from Eq.(15) for a modulation frequency ω = 0.2 Hz. The predicted sample motion is shown in the upper trace of figure 4-1.(a). As expected, the equilibrium levitation position increased after application of the modulation power. In addition, the sample is predicted to oscillate about the equilibrium position in phase and at the same frequency as the power modulation frequency.

The theoretical thermal response of the upper pole of the spherical sample to the modulated input power is shown in figure 4-1.(b). The thermal response of the upper pole also displays the same frequency as the modulation power. Peak temperatures were predicted to occur at the equator as expected. In addition, the sample exhibited slightly smaller temperature amplitudes for the motionless condition as shown in the figure 4-1.(b), and the difference between the motionless and moving sample cases is about 2.1%.

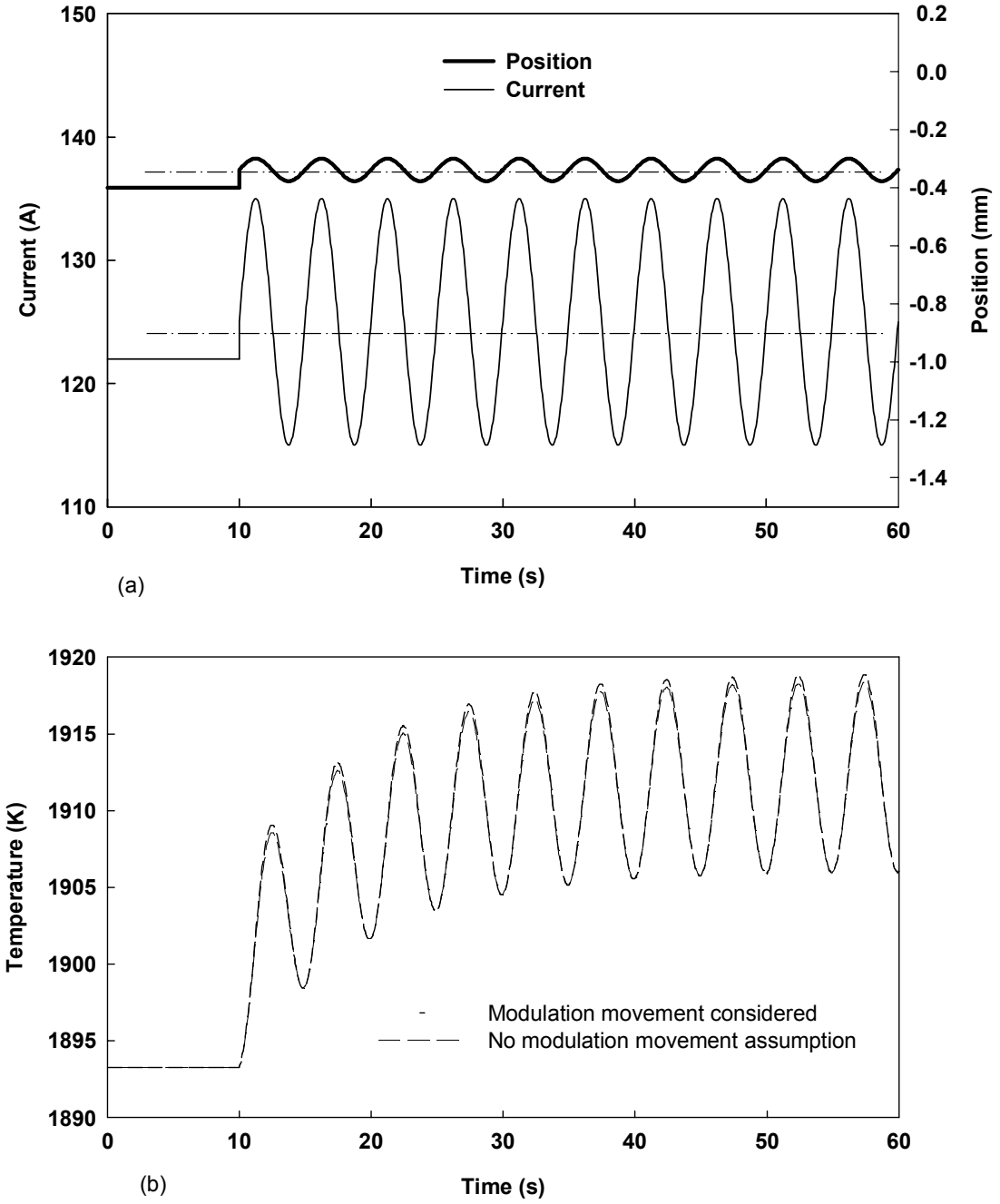

Figure 4-1. (a) The peak coil current (lower trace) and resultant sample position response (upper trace). (b) Comparison of dynamic temperature response of the sample for motionless and moving sample cases. ω= 0.2 Hz, I_o=122 A, ΔI_o=3 A, I_m=10 A.

4.2. Thermal Expansion of Molten Nickel and Nickel-Based Alloy IN713

In order to test the accuracy of the present image processing technique, two different diameter steel calibration balls (AISI E52100) were electromagnetically heated, and the images were recorded from the video camera and analyzed for their volumes. The composition of AISI E52100 steel is summarized in Table 4-1.

Table 4-1. AISI E52100 steel composition (wt %).

Element	C	Cr	Fe	Mn	P	S	Si
E52100	0.98-1.1	1.45	97	0.35	Max 0.025	Max 0.025	0.23

The normalized volumes (value divided by the average value) are shown in figure 4-2. Figure 4-2(a) shows the volume measurements using the improved threshold method, and figure 4-2 (b) shows the volume measurements using the maximum intensity gradient method. The result shows that the improved threshold method exhibits a smaller standard deviation in terms of volume determination. The difference in these two methods arises mainly from the blooming effect, which generated a noisy contour for the heated, bright calibration balls. Figure 4-3 shows the density of the calibration balls based on the volume determination using the two imaging processing techniques. Compared with the literature reference (Esser and Eusterbrock, 1941), the result shows that the improved threshold method agrees well with the reference values. The maximum intensity gradient method reveals a tendency to overestimate the sample's volume and lead to a smaller density value in agreement with blooming effects.

The density of a molten nickel sample (99.99% purity) was evaluated from a set of image data using the two image analysis techniques. These data were then compared to

density data from Chung et al.(1996). In that previous work, a very stable electrostatic levitator was used to eliminate image degradation from sample translation effects and backlighting of the sample eliminated noisy image data from CCD blooming effects. The data of Chung et al. exhibited minimum scatter and is believed to accurately represent the density of molten nickel. Figure 4-4 shows data of the density of molten nickel from the present investigation using the maximum intensity gradient method and the improved threshold method as well as the literature (Chung et al., 1996). The result for the liquid phase density can be expressed by

Maximum intensity gradient method:

$$\rho \text{ (g/cc)} = 9.5296 - 0.0010*T \quad \text{(K)} \tag{31}$$

Improved threshold method:

$$\rho \text{ (g/cc)} = 8.7726-0.0005*T \quad \text{(K)} \tag{32}$$

Reference (Chung et al., 1996):

$$\rho \text{ (g/cc)} = 9.0391-0.0007*T \quad \text{(K)} \tag{33}$$

The maximum intensity gradient method does not provide as good an agreement with the prior work (Chung et al., 1996) as does the threshold method for direct images from bright, glowing samples, presumably due to CCD blooming effects. CCD blooming biases the maximum intensity gradient method towards larger estimates of sample sizes and consequently lower densities. Although CCD blooming effects can be eliminated by backlighting the sample, backlighting does introduce additional instrument complexity. The pixel threshold method essentially solves this problem by “calibrating” the blooming effect through measurement of the known coil diameter and establishing the correct threshold pixel value for a bright edge against a dark background. Note that the deviation

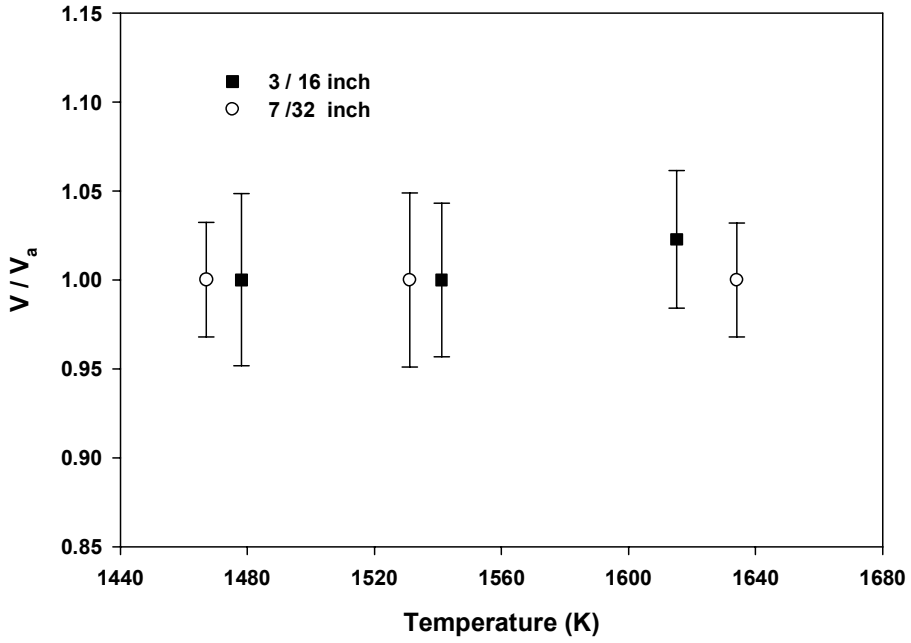

(a)

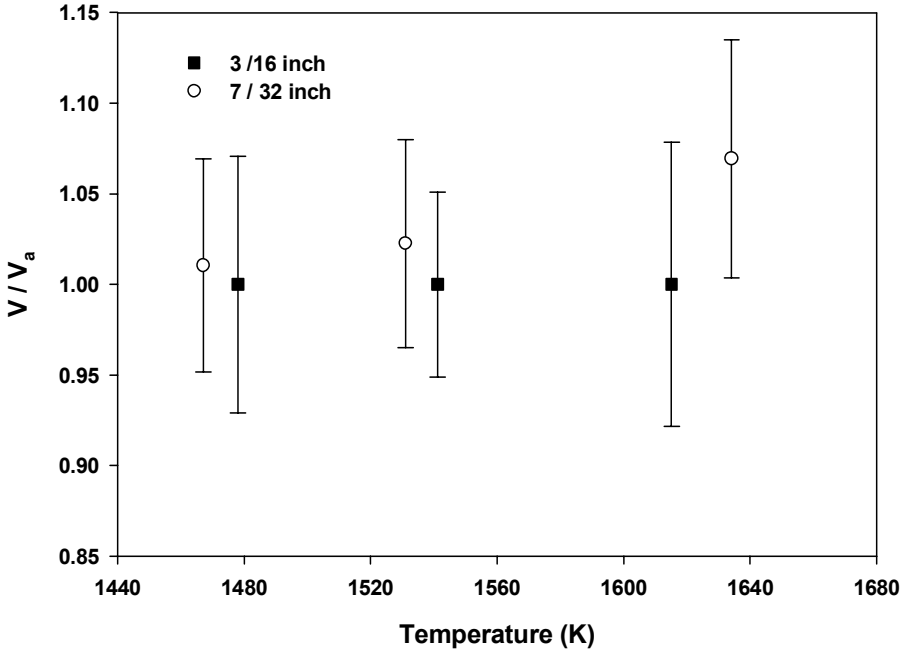

(b)

Figure 4-2. Volume measurements of two steel calibration balls using image processing (a) improved threshold method and (b) maximum intensity gradient method.

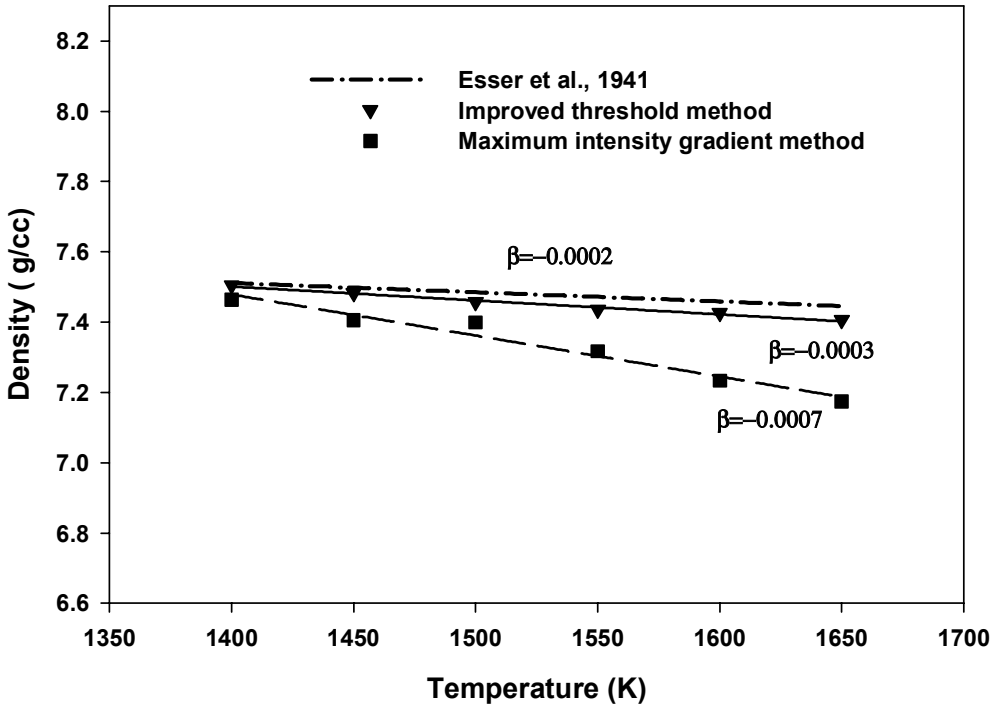

Figure 4-3. Density of the steel calibration balls.

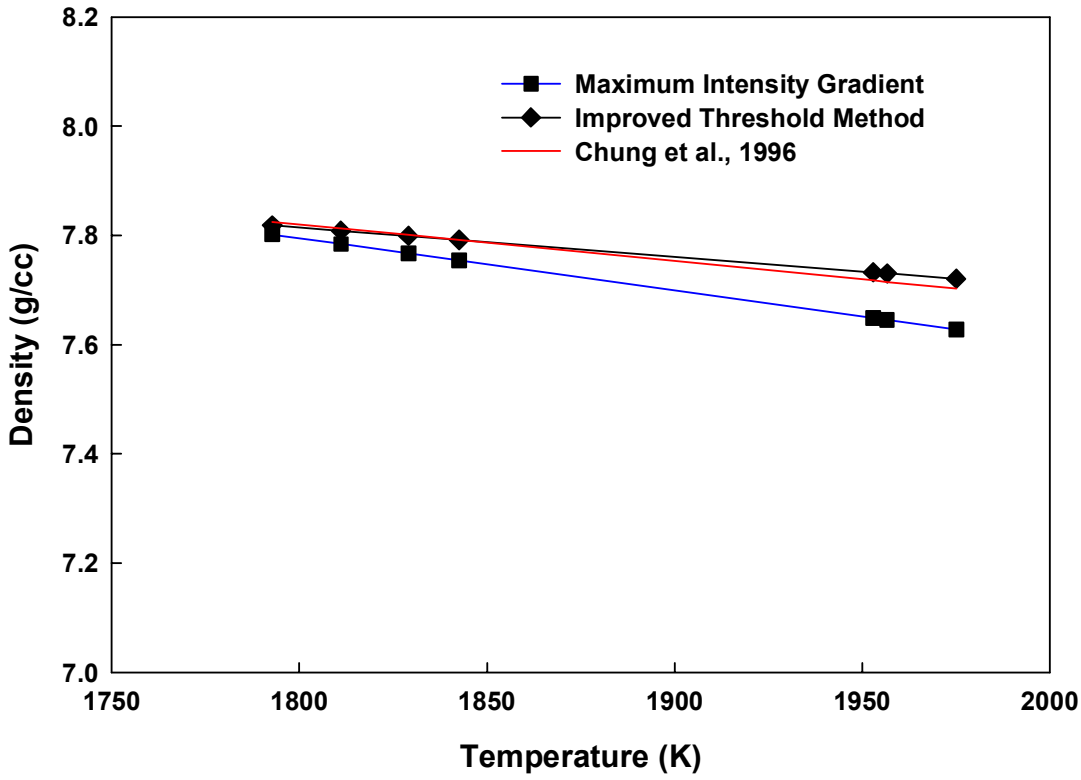

Figure 4-4. Experimentally determined density of electromagnetically levitated liquid nickel sample.

of the maximum gradient method increases as the temperature of the nickel sample increases, presumably due to increased CCD blooming from the brighter samples.

Commercial nickel-based superalloy IN713 is widely used in demanding applications due to the alloy's excellent high temperature strength. The composition of this alloy is shown in Table 4-2.

Table 4-2. Nickel-based superalloy IN713 composition (wt %).

Element	C	Cr	Mo	Fe	Ti	Al	Co	Nb
IN713	0.13	13.89	4.0	0.2	0.9	6.0	0.15	2.0

Unfortunately electromagnetic levitation of such alloys is difficult because the electrical conductivities are low and the densities are high. Successful levitation and melting of the alloy was achieved after several different coil designs were tested. Volumes of the samples were estimated using the image threshold technique. The sample masses were measured before and after the experiments and the sample mass during the measurements estimated assuming constant evaporation rates while each sample was molten. The measured density of IN713 in liquid state with 95% prediction interval of the regression line is shown in Figure 4-5.

4.3. Modulated Power Specific Heat Measurements

Modulation heating and cooling experiments were performed with solid nickel, titanium and zirconium samples in the temperature range of 1300 K to 1800 K. The samples were suspended in the center of the induction coil with a very small 0.15 mm diameter Pt (87%)-Rh (13%) wire.

A simple conduction model of the heat losses through the wire was developed by

assuming that one end of the Pt-Rh wire is held at the sample temperature and the other end of the wire is held at room temperature. The results are shown in figure 4-6 and suggests that the heat losses through the wire varied from about 1.5% of the radiation losses at 1273 K to around 0.5% of the radiation losses at 1773 K for a 6 mm diameter nickel sample.

The thermal response of the suspended samples were evaluated after being heated to four steady state temperatures and then subjected to a sinusoidally-modulated heating power. The total hemispherical emissivity of the samples were determined from the spectral normal emissivity measurement by coupling a FTIR spectrometer with the electromagnetic levitator (Teodorescu et al., 2005). The sample's specific heat was then calculated from the measurements of T_o and ΔT_ω using the methodology described above, i.e., Eqs. (14, 21, and 22). The measurements were performed for each material using two samples with different diameters as noted in the figures. The reproducibility of measurements for individual samples was ±3%.

The heat capacity measurement of nickel is shown in Fig.4-7. There is general agreement between the present results and the data of Booker et al.(1961), Cezairliyan and Muelle (1983), Desai (1987), and Krauss and Warncke (1955). Figure 4-8 shows that the experimentally determined heat capacity of titanium from the present work agrees with Maglic et al.(2001), Kaschnitz et al. (2001)and Paradis et al. (2000) up to approximately 1600 K. The present data indicate lower heat capacity values than the literature values in the 1600-1700 K temperature range. Additional testing is required to better understand the reason for this difference. Figure 4-9 shows that the experimentally determined heat capacity of zirconium from the present work is in good agreement with Hultgren et al (1973) and the pulse heating experiments reported by Cezairliyan et

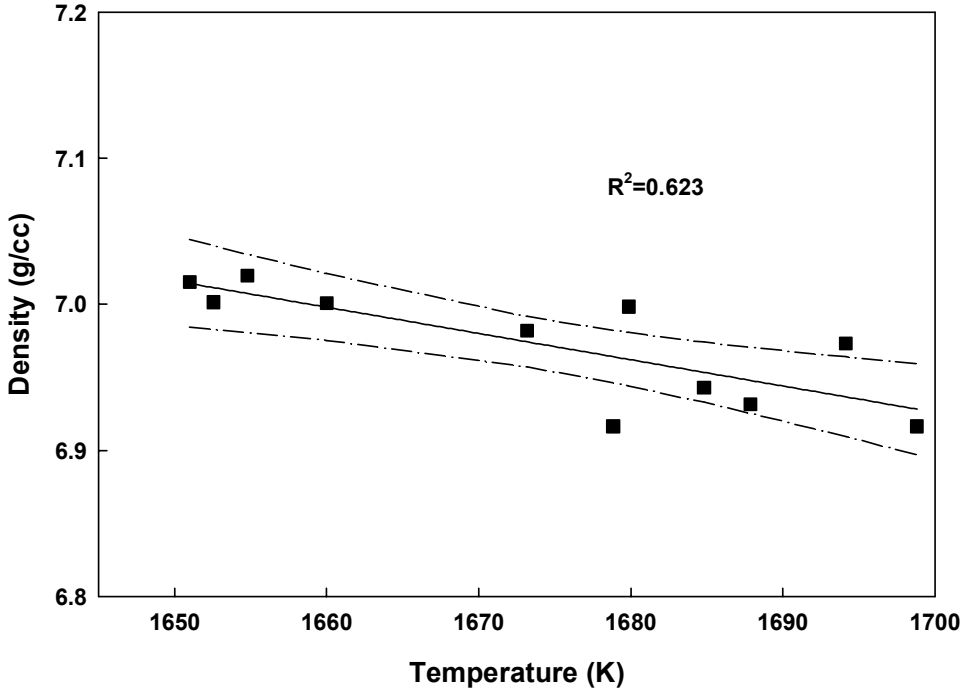

Figure 4-5. Experimentally determined density of electromagnetically levitated molten IN713.

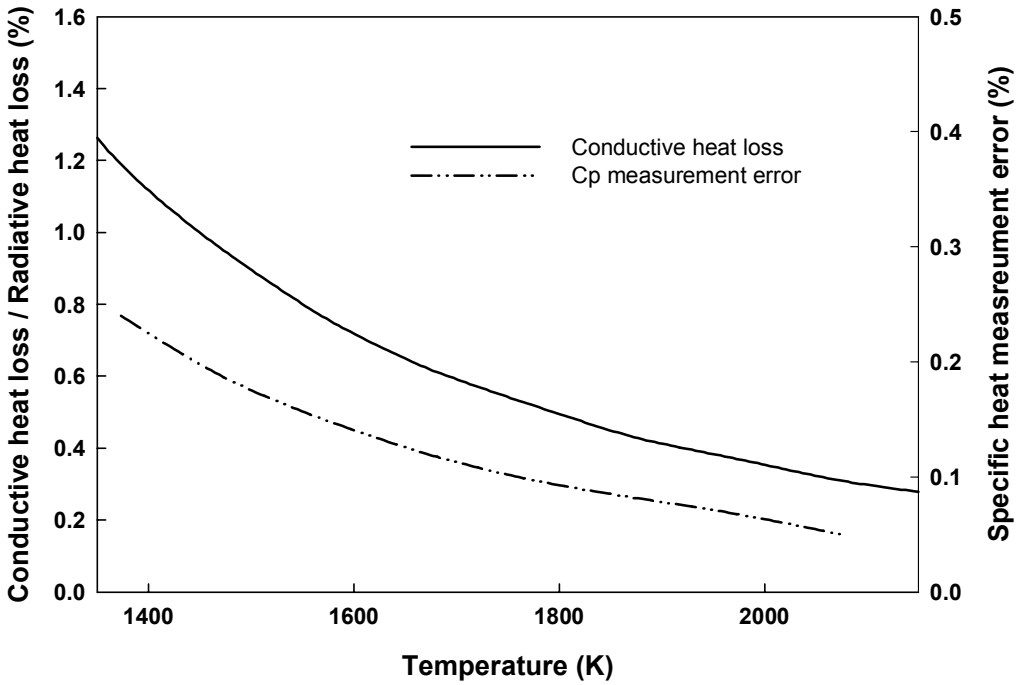

Figure 4-6. Conductive heat loss through the suspension wire and its effect on heat capacity calculation.

al.(1974). Alcock et al. (1976) reported slightly higher values of the heat capacity as well as greater temperature dependence.

The least-squares fit polynomial functions that represent the results for heat capacity for nickel, titanium and zirconium in the measured temperature range are:

Nickel: ($1380 \le T \le 1678$)

$$C_p = 61.885 - 0.109 \times \mathrm{T} + 1.050 \times 10^{-4} \times T^2 - 2.923 \times 10^{-8} \times T^3 \qquad (34)$$

Titanium: ($1361 \le T \le 1721$)

$$C_p = 75.767 + 0.190 \times \mathrm{T} - 1.112 \times 10^{-4} \times T^2 + 2.194 \times 10^{-8} \times T^3 \qquad (35)$$

Zirconium: ($1359 \le T \le 1686$)

$$C_p = 121.315 - 0.201 \times \mathrm{T} + 1.442 \times 10^{-4} \times T^2 - 3.341 \times 10^{-8} \times T^3 \qquad (36)$$

where C_p is in $\mathrm{J \cdot mol^{-1} \cdot K^{-1}}$, and T is in K. In the computation of heat capacity, the atomic weights of nickel, titanium and zirconium were taken as 58.693, 47.880 and 91.224, respectively.

Moffat's uncertainty estimation procedure (Moffat, 1998) was used to theoretically analyze the various contributions to the experimental uncertainty. The results of these calculations are shown in Table 4-3, 4-4, and 4-5. The total estimated uncertainty (95% confidence limits) is approximately 4.5 % for a typical specific heat measurement.

The largest contributor to the uncertainty in specific heat measurement was the uncertainty in emissivity (primarily due to the ±0.5% uncertainty in temperature measurement of the noncontact pyrometer). Improvements in the accuracy of the temperature characterization are possible on measurements of solid samples of pure elements evaluated incrementally just below and just above the melting temperature.

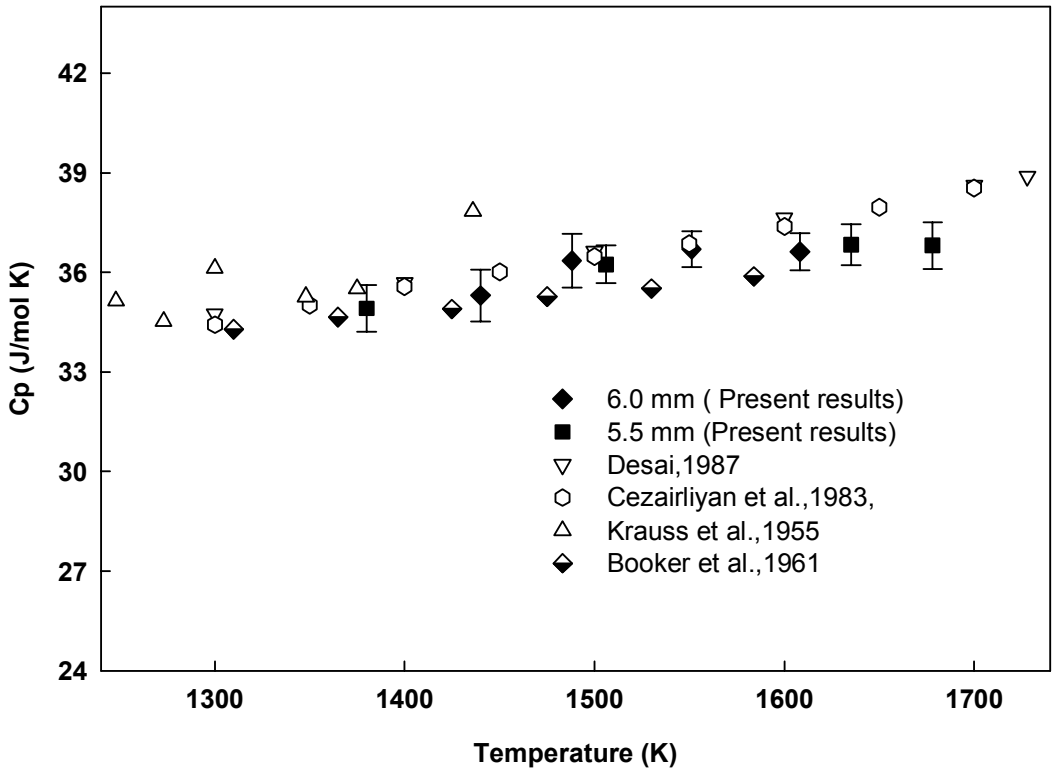

Figure 4-7. Heat capacity of nickel: present work and data reported in the literature.

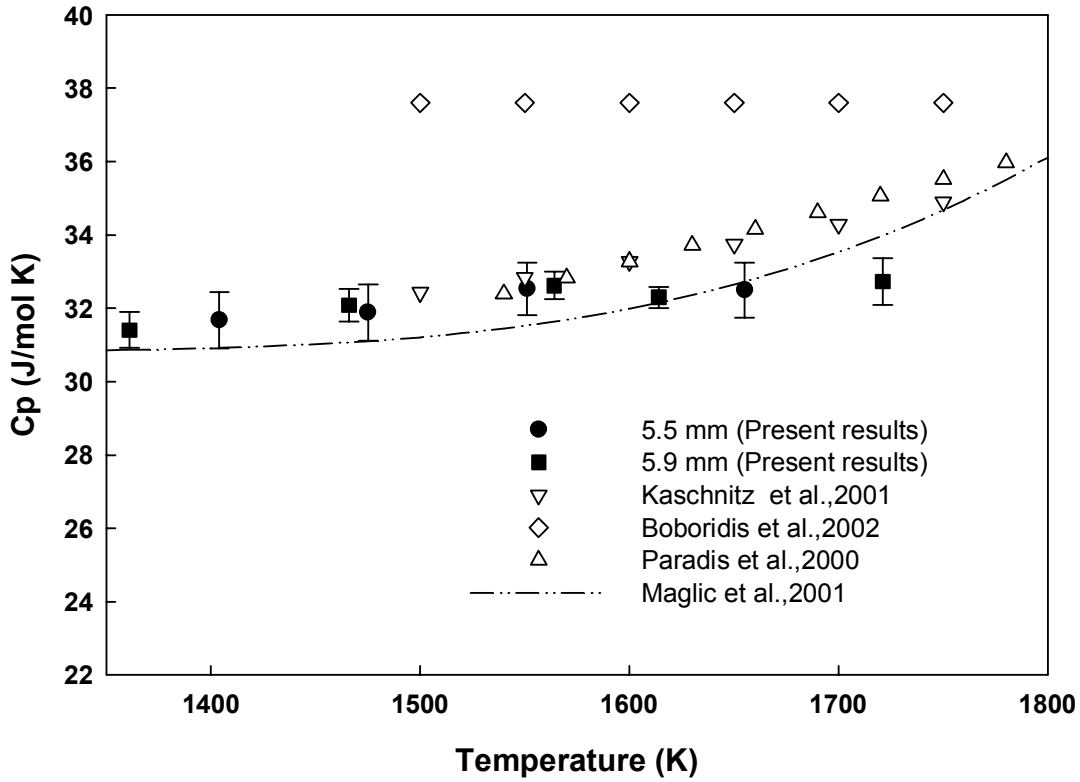

Figure 4-8. Heat capacity of titanium: present work and data reported in the literature.

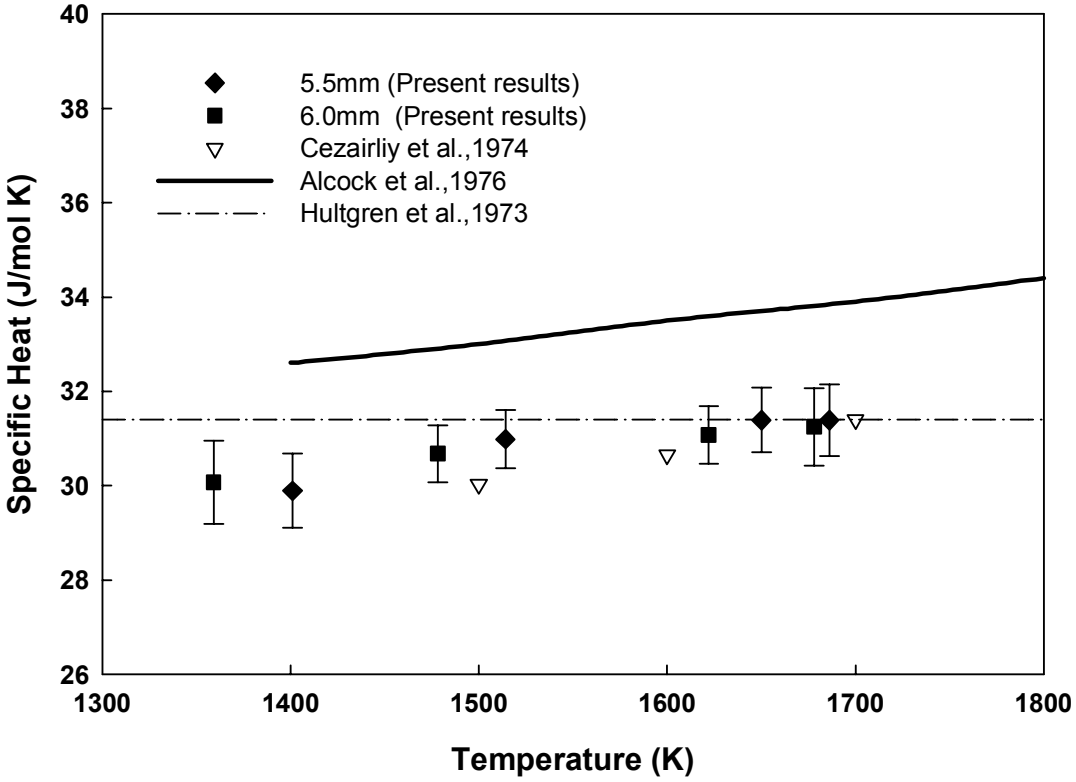

Figure 4-9. Heat capacity of zirconium: present work and data reported in the literature.

Table 4-3. Uncertainty Estimates of the Nickel Specific Heat Measurement using the EML Modulated Power Method.

Parameter	Estimated ±2σ confidence limits (%)	Specific heat change (J/mol K)	Specific heat change squared $(J/mol\ K)^2$
Temperature T=1500(K)	0.5	0.72	0.51
Modulation frequency ω=0.2(Hz)	0.2	0.07	0.005
Sample mass m=945 (mg)	0.1	0.04	0.001
Temperature amplitude ΔT_m=5(K)	0.5	0.18	0.032
DC control voltage V_o= 80 (V)	0.2	0.07	0.005
AC control voltage V_m=21.8(V)	0.2	0.03	0.001
Emissivity ε=0.2	4.0	1.43	2.05
Total uncertainty in specific heat, J/mol K $[\Sigma(\Delta\mu_i)^2]^{1/2}$			1.61
Total % uncertainty in specific heat (35.80 J/mol K)			±4.5%

Table 4-4. Uncertainty Estimates of the Titanium Specific Heat Measurement using the EML Modulated Power Method.

Parameter	Estimated ±2σ confidence limits (%)	Specific heat change (J/mol K)	Specific heat change squared $(J/mol\ K)^2$
Temperature T=1500(K)	0.5	0.648	0.420
Modulation frequency ω=0.2(Hz)	0.2	0.065	0.004
Sample mass m=710 (mg)	0.1	0.033	0.001
Temperature amplitude ΔT_m=8 (K)	0.5	0.162	0.026
DC control voltage V_o=98(V)	0.2	0.065	0.004
AC control voltage V_m=12 (V)	0.2	0.035	0.001
Emissivity ε=0.28	4.0	1.294	1.674
Total uncertainty in specific heat, J/mol K $[\Sigma(\Delta\mu_i)^2]^{1/2}$			1.46
Total % uncertainty in specific heat (32.31J/mol K)			±4.52%

Table 4-5. Uncertainty Estimates of the Zirconium Specific Heat Measurement using the EML Modulated Power Method.

Parameter	Estimated ±2σ confidence limits (%)	Specific heat change (J/mol K)	Specific heat change squared $(J/mol\ K)^2$
Temperature T=1500(K)	0.5	0.561	0.315
Modulation frequency ω=0.2(Hz)	0.2	0.056	0.003
Sample mass m=484 (mg)	0.1	0.028	0.001
Temperature amplitude ΔT_m=10(K)	0.5	0.140	0.020
DC control voltage V_o=90(V)	0.2	0.056	0.003
AC control voltage V_m=21.8(V)	0.2	0.039	0.002
Emissivity ε=0.27	4.0	1.121	1.256
Total uncertainty in specific heat, J/mol K $[\Sigma(\Delta\mu_i)^2]^{1/2}$			1.27
Total % uncertainty in specific heat (30.29 J/mol K)			± 4.21%

5. CONCLUSIONS

This work includes two general parts: (i) thermal expansion measurements and (ii) heat capacity measurements in the earth-based electromagnetic levitator of Auburn University.

For thermal expansion measurements, CCD blooming effects from the emitted radiation of electromagnetically levitated samples can cause noisy image data and decreased precision in measurements of sample size using the traditional maximum intensity gradient method. However, the presence in the image of the water cooled copper coil presents a convenient image of known size to establish the threshold pixel intensity value for the edge for each picture and enables effective calibration of the image for the blooming effect. These image-specific pixel threshold values can then be used to determine the molten droplet edges. Sixth order Legendre polynomials can then be fit to the droplet edge data to obtain accurate and precise measurements of the sample volume assuming that axisymetric symmetry prevails. The method was confirmed with measurements on precision steel calibration balls and pure nickel and then applied to measurements of the density of IN713.

The modulation power method combined with electromagnetic levitation high temperatures, especially when interactions with the crucible and contamination are concerns. The largest contributor to the uncertainty in specific heat is the uncertainty in total hemispherical emissivity values used to calculate the radiative power losses. The

method was successfully applied to measure the heat capacity of pure solid samples of nickel, titanium and zirconium suspended on a thin Pt-Ph wire. Although the coupled heating power and positioning force for the traditional single coil electromagnetic levitator design introduces cyclic translations of the sample, these effects are predicted by a numerical model developed in this study to have negligible affect on the measurements.

6. SUGGESTIONS FOR FUTURE RESEARCH

To improve accuracy of the density and heat capacity measurements, the current experimental system can be modified in the following ways:

The current optical system and temperature measurement system performance can be significantly improved by reducing the electromagnetic noise generated by the RF power supply.

Placing the current CCD camera with a higher resolution CCD camera will improve the resolution of image sizes.

The modulated power method may also be applied to monitoring the phase transformation and measuring the alloy's latent heat. Application of the modulated power method within the mushy zone of an alloy will cause periodic melting and freezing processes and induce additional lag in the thermal response of the sample. Measurements of an alloy's specific heat over the range of temperatures associated with the phase transformation will produce heat capacity measurements above the baseline expected for a single phase. When this apparent heat capacity is plotted versus temperature, a peak will naturally result and indicate the phase transformation. Integration of the apparent heat capacity curve above the single phase baseline will yield the transformation enthalpy.

REFERENCES

Alcock, C. B.; Jacob, K. T. and Zador, S., "Thermochemical properties [of zirconium]", Atomic Energy Review, Special Issue, vol.6, pp.7-65, 1976

Bachmann, R.; DiSalvo, F. J., Jr.; Geballe, T. H.; Greene, R. L.; Howard, R. E.; King, C. N.; Kirsch, H. C.; Lee, K. N.; Schwall, R. E. and et al., "Heat capacity measurements on small samples at low temperatures", Review of Scientific Instruments, vol.43 (2), pp.205-214, 1972

Bakhtiyarov, S. I. and Overfelt, R. A., "Thermophysical property measurements by electromagnetic levitation melting technique under microgravity", Annals of the New York Academy of Sciences, vol.974, pp.132-145, 2002

Bakhtiyarov, S. I. and Overfelt, R. A., "Electromagnetic levitation: Theory, experiments, application", Recent Research Developments in Materials Science, vol.4 (Pt. 1), pp.81-123, 2003

Boboridis, K., "Thermophysical property measurements on niobium and titanium by a microsecond-resolution pulse-heating technique using high-speed laser polarimetry and radiation thermometry", International Journal of Thermophysics, vol.23 (1), pp.277-291, 2002

Booker, J.; Paine, R. M. and Stonehouse, A. J., "Intermetallic compounds for very high temperature applications", United States Department of Commerce, Office of Technical Services, AD [ASTIA Document], 1961

Brandes, E. A. and Brook, G. B., "Smithells Metals Reference Book", Butterworths – Heinemann Ltd, Oxford, vol.8, pp.54-55, 1992

Brillo, J. and Egry, I., "Density Determination of Liquid Copper, Nickel, and Their Alloys", International Journal of Thermophysics, vol.24 (4), pp.1155-1170, 2003

Cezairliyan, A. and Mueller, A. P., "Heat capacity and electrical resistivity of nickel in the range 1300-1700 K measured with a pulse heating technique", International Journal of Thermophysics, vol.4 (4), pp.389-396, 1983

Cezairliyan, A. and Righini, F., "Simultaneous measurements of heat capacity, electrical resistivity, and hemispherical total emittance by a pulse heating technique. Zirconium 1500 to 2100.deg. K", Journal of Research of the National Bureau of Standards, Section A: Physics and Chemistry, vol.78 (4), pp.509-514, 1974

Chen, S. F. and Overfelt, R. A., "Effects of sample size on surface-tension measurements of nickel in reduced-gravity parabolic flights", International Journal of Thermophysics, vol.19, pp.817-826, 1998

Chung, S. K.; David, B. T. and Won-kyu, R., "A noncontact measurement technique for the density and thermal expansion coefficient of solid and liquid materials", Review of Scientific Instruments, vol.67 (9), pp.3175-3181, 1996

Damaschke, B.; Oelgeschlaeger, D.; Ehrich, J.; Dietzsch, E. and Samwer, K., "Thermal expansion measurements of liquid metallic samples measured under microgravity conditions", Review of Scientific Instruments, vol.69 (5), pp.2110-2113, 1998

Desai, P. D., "Thermodynamic properties of nickel", International Journal of Thermophysics, vol.8 (6), pp.763-780, 1987

Egry, I.; Diefenbach, A.; Dreier, W. and Piller, J., "Containerless processing in space -

Thermophysical property measurements using electromagnetic levitation", International Journal of Thermophysics, vol.22 (2), pp.569-578, 2001

Egry, I.; Lohoefer, G. and Sauerland, S., "Measurements of thermophysical properties of liquid metals by noncontact techniques", International Journal of Thermophysics, vol.14 (3), pp.573-584, 1993

El-Mehairy, A. E. and Ward, R. G., "A new technique for determination of density of liquid metals: application to copper", Transactions of the American Institute of Mining, Metallurgical and Petroleum Engineers, vol.227 (5), pp.1126-1128, 1963

Esser, H. and Eusterbrock, H., "Investigation of the thermal expansion of some metals and alloys with an improved dilatometer", Archiv fuer das Eisenhuettenwesen, vol.14, pp.341-355, 1941

Fecht, H.-J. and Johnson, W. L., "A conceptual approach for noncontact calorimetry in space", Review of Scientific Instruments, vol.62(5), pp.1299-1303, 1991

Fecht, H.-J. and Wunderlich, R. K., "Development of containerless modulation calorimetry for specific heat measurements of undercooled melts", Materials Science & Engineering, A: Structural Materials: Properties, Microstructure and Processing, vol.178 (1-2), pp.61-64, 1994

Fromm, E. and Jehn, H., "Electromagnetic Forces and Power Absorption in Levitation Melting", British Journal of Applied Physics, vol.16, pp.653-663, 1965

Gonzalez, R. C. and Wintz, P. A., "Digital Image Processing", pp.331-391, 1987

Gorges, E.; Racz, L. M.; Schillings, A. and Ergy, I., "Density measurements on levitated liquid metal droplets", International Journal of Thermophysics, vol.17 (5), pp.1163-1172, 1996

Herlach, D. M.; Cochrane, R. F.; Egry, I.; Fecht, H. J. and Greer, A. L., "Containerless processing in the study of metallic melts and their solidification", International Materials Reviews, vol.38 (6), pp.273-347, 1993

Hultgren, R. and et al. (1973). Selected Values of the Thermodynamic Properties of the Elements.

Jain, A. K., "Fundamental of Digital Image Processing", pp. 407-414, 1989

Kaschnitz, E. and Reiter, P., "Heat capacity of titanium in the temperature range 1500 to 1900 K measured by a millisecond pulse-heating technique", Journal of Thermal Analysis and Calorimetry, vol.64 (1), pp.351-356, 2001

Krauss, F. and Warncke, H., "Specific heat of nickel between 180 and 1160 Deg", Zeitschrift fuer Metallkunde, vol.46, pp.61-69, 1955

Maglic, K. D. and Pavicic, D. Z., "Thermal and electrical properties of titanium between 300 and 1900 K", International Journal of Thermophysics, vol.22 (6), pp.1833-1841, 2001

Moffat, R. J., "Describing the Uncertainties in Experimental Results", Exp. Therm Fluid Science, vol.1, pp.3-17, 1998

Ohsaka, K.; Holzer, J. C.; Trinh, E. H. and Johnson, W. L., "Specific heat measurement of undercooled liquids", 4th International conference on experiment methods for microgravity materials science research, pp.1-6, 1992

Okress, E. C.; Wroughton, D. M.; Comentz, G.; Brace, P. H. and R.Kelly, J. C., "Electromagnetic Levitation of Solid and Molten Metals", Journal of Applied Physics, vol.23, pp.545 - 552, 1952

Paradis, P.-F. and Rhim, W.-K., "Non-contact measurements of thermophysical properties

of titanium at high temperature", Journal of Chemical Thermodynamics, vol.32 (1), pp.123-133, 2000

Racz, L. M. and Egry, I., "Advances in the measurement of density and thermal expansion of undercooled liquid metals", Review of Scientific Instruments, vol.66 (8), pp.4254-4258, 1995

Schaefers, K.; Rösner-Kuhn, M. and Frohberg, M. G., "Enthalpy measurements of undercooled metals by levitation calorimetry: the pure metals nickel, iron, vanadium and niobium", Materials Science and Engineering, vol. A 197, pp.83-90, 1995

Sullivan, P. F. and Seidel, G., "Steady-state, a.c.-temperature calorimetry", Physical Review, vol.173 (3), pp.679-685, 1968

Teodorescu, G.; Jones, P. D.; Overfelt, R. A. and Guo, B., "Spectral-normal Emissivity of Electromagnetic Heated Ni at High Temperature", Materials Science & Technology Conference and Exhibition, Pittsburgh, PA, Sept 25-28, 2005

Wang, D.; Guo, B. and Overfelt, R. A., "Surface tension measurements of cast irons by electromagnetic levitation melting technique", AFS Transactions, vol.111, pp.813-824, 2003

Wroughton, D. M.; Okress, E. C.; Brace, P. H.; Comenetz, G. and Kelly, J. C. R., "A technique for eliminating crucibles in heating and melting metals", Journal of the Electrochemical Society, vol.99, pp.205-211, 1952

Wunderlich, R. K.; Diefenbach, A.; Willnecker, R. and Fecht, H. J., "Principles of non-contact a.c. calorimetry", Containerless Process.: Tech. Appl., Proc. Int. Symp. Exp. Methods Mater. Sci. Res., 5th, pp.51-56, 1993

Wunderlich, R. K.; Ettl, C. and Fecht, H.-J., "Non-contact electromagnetic calorimetry of metallic glass forming alloys in reduced gravity", ESA SP, vol.454I, pp.537-544, 2000

Wunderlich, R. K.; Ettl, C. and Fecht, H. J., "Non-contact electromagnetic calorimetry of metallic glass forming alloys in reduced gravity", European Space Agency, [Special Publication] SP, vol. SP-454 (Vol. 1, First International Symposium on Microgravity Research & Applications in Physical Sciences and Biotechnology, 2000, Volume 2), pp.537-544, 2001

Wunderlich, R. K.; Ettl, C. and Fecht, H. J., "Specific heat and thermal transport measurements of reactive metallic alloys by noncontact calorimetry in reduced gravity", International Journal of Thermophysics, vol.22 (2), pp.579-591, 2001

Wunderlich, R. K. and Fecht, H. J., "Specific heat measurements by non-contact calorimetry", Journal of Non-Crystalline Solids, vol.156-158 (Pt. 1), pp.421-424, 1993

Wunderlich, R. K. and Fecht, H. J., "Measurements of thermophysical properties by contactless modulation calorimetry", International Journal of Thermophysics, vol.17 (5), pp.1203-1216, 1996

Wunderlich, R. K.; Lee, D. S.; Johnson, W. L. and Fecht, H. J., "Noncontact modulation calorimetry of metallic liquids in low earth orbit", Physical Review B: Condensed Matter, vol.55 (1), pp.26-29, 1997

Xuan, X., "Levitation and Surface Tension Measurement of Materials by Electromagnetic levitation", M.S. thesis, Auburn University, pp.12-27, 2000

APPENDIX A

THE SOURCE CODE FOR THERMAL EXPANSION MEASUREMENT

```
% Main program is designed coil measurement
% function   xycenter:   for center detection
% function   intens: for characteristic intensity detection
clc;
clear;
% function    coil:   for coil detection
% function    radius:   for edge detection
 SS=31;    % The first Picture
 MM=40;    % The last Picture
 for NN=SS:MM,
    cd('U:\In713 April 26');
    s1=char('p');
    s11=char('coil');
    s2=int2str(NN);
    s3=char('.jpg');
    name=strcat(s1,s2,s3)         % Image file: pX.jpg
    datafile=strcat(s11,s2);    % Data   file: cedgeX
    I=imread(name);
    cd('H:\Program');
    A=rgb2gray(I);
    corner1=[65,220];
    corner2=[1092,1020];
    xleft=corner1(1);
    yupp=corner1(2);
    xright=corner2(1);
    ydownp=corner2(2);
    A=A(yupp:ydownp,xleft:xright);
    B= im2double(A);
    [m,n]=size(B);
    % Find the characteristic intensity
    % Coil Region
     mark1=100;
     mark2=150;
     mark3=210;
% Center Position determination
[centerx,centery]=xycenter(B,mark1,mark3);
[cyupc,cydownc,coillength,transion]=
      coil(B,centerx,mark1,mark2,mark3);
      cd('H:\Program\Data\Coil');
      save(datafile, 'cyupc','cydownc','centerx','centery','coillength');
    clc;
    clear;
end
% Sub_program
function [centerx,centery]= xycenter(B,mark1,mark3)
```

```
[m,n]=size(B);
exline=B(mark1,:);
[record,index]=max(exline);
exline1=[index,1];
exline2=[index,n];
eyline=[mark1,mark1];
[cx1,cy1,c1]=improfile(B,exline1,eyline,'bicubic');
[cx2,cy2,c2]=improfile(B,exline2,eyline,'bicubic');
recordl=0;
critical=0.46;
intensity=record-critical*(record-recordl);
hh=1;
    while c1(hh)>intensity,
              hh=hh+1;
    end
x1=cx1(hh);
in1=c1(hh);     % Left edge point
       hh=1;
       while c2(hh)>intensity, %
           hh=hh+1;
       end
       x2=cx2(hh);
       in2=c2(hh);     %%% Right edge point
       xcenter=(x1+x2)/2;
       centerx=round(xcenter);
       xcenter=centerx;
       % Center y determination
       eyline=B(:,xcenter);
       [record,index]=max(eyline);
       intensity=record-critical*(record-recordl);
       exline=[xcenter,xcenter];
       eyline1=[mark1,1];
       eyline2=[mark3,m];
       hh=1;
       [cx1,cy1,c1]=improfile(B,exline,eyline1,'bicubic');
       [cx2,cy2,c2]=improfile(B,exline,eyline2,'bicubic');
        while c1(hh)>intensity,
            hh=hh+1;
        end
       y1=cy1(hh);   % Upper edge point
       in1=c1(hh);
       hh=1;
% For some reason: the mist in the image, we can only use maximum intensity gradient to
find the ycenter position
    recordl=min(c2);
```

```
    if recordl<intensity,
        while c2(hh)>intensity,
            hh=hh+1;
        end
        y2=cy2(hh); % Lower edge point
      in2=c2(hh);
    else
         dif=-diff(c2);
      [record,index]=max(dif);
      y2=cy2(index);
      in2=c2(index);
    end

      ycenter=(y1+y2)/2;
      ycenter=round(ycenter);
      centery=ycenter;
%-----------------------------------------------

clc;
clear;
% This program is designed for the correction factor of every group images and the highest
intensity of the image
SS=11;          % The start Picture
MM=30;          % The final Picture
ww=188.0346; % coil distance
for NN=SS:MM,
  cd('H:\Program\Sample image\In718 April06(2)');
  s1=char('p');
  s11=char('coren');
  s2=int2str(NN);
  s3=char('.jpg');
  name=strcat(s1,s2,s3)         % Image File
  datafile=strcat(s11,s2);    %   Data File
  I=imread(name);
   cd('H:\Program');
   A=rgb2gray(I);
   corner1=[65,220];
   corner2=[1092,1020];
   xleft=corner1(1);
   yupp=corner1(2);
   xright=corner2(1);
   ydownp=corner2(2);
   A=A(yupp:ydownp,xleft:xright);
   B= im2double(A);
   [m,n]=size(B);
```

```
    % Coil Region
     mark1=480;
     mark2=600;
     mark3=705;
[centerx,centery]=xycenter(B,mark1,mark3);
  recordh=intens(B,centerx);
  recordl=0;
   critical=0.6;
    ww=188.0346;
    % Center Line Improfile
  xline=[centerx,centerx];
  yline1=[mark1,mark2];
  yline2=[mark3,mark2];
  [cxc1,cyc1,cc1]=improfile(B,xline,yline1,'bicubic');
  [cxc2,cyc2,cc2]=improfile(B,xline,yline2,'bicubic');
  [recordup,indexhup]=max(cc1);
  [recorddown,indexdown]=max(cc1);
  recordl=0;
  ccoil=0;
while abs(ccoil-ww)>2 & critical>=0.20,
  intensityup=recordh-critical*(recordh-recordl);
  intensitydown=recordh-critical*(recordh-recordl);
   % Searching the upper and lower level
  indexup=1;
  while cc1(indexup)>intensityup,
          indexup=indexup+1;
  end
  indexdown=1;
  while cc2(indexdown)>intensitydown,
          indexdown=indexdown+1;
  end
  cyupc=cyc1(indexup);          % Up edge of coil
  cydownc=cyc2(indexdown);     % Low edge of coil
  ccoil=cydownc-cyupc;          %Coil distance
  critical=critical-0.01;
end
cd('H:\Program\Data\Core');
save(datafile, 'critical','ccoil','recordh');
       clc;
       clear;
end
function intensity=intens(B,centerx)
  for h=1:10,
      exline=B(:,centerx);
      inten(h)=max(exline);
```

```
   end
   intensity=mean(inten);
clear;
clc;
% read critical value function
SS=21;          % The start Picture
MM=25;          % The final Picture
h=1;
for NN=SS:MM,
   cd('H:\Program\Data\Core');
   s11=char('coren');
   s2=int2str(NN);
   datafile=strcat(s11,s2);     % Data File
   load(datafile);
   value(h)=critical;
   data(h)=ccoil;
   intensity(h)=recordh;
   edgein(h)=intensity(h)*(1-value(h));
   h=h+1;
end
end
%

% This program is designed for edge detection
% function      xycenter:   for center detection
% function      intens   : for characteristic intensity detection
clc;
clear;
%% function          coil      :   for coil detection
%% function          radius   :   for edge detection
%-------------------------------------------------------
 SS=21;         % The first Picture
 MM=25;         % The last Picture
for NN=SS:MM,
    critical=0.31;
    s1=char('p');
    s11=char('cedgenew');
    s2=int2str(NN);
    s3=char('.jpg');
    name=strcat(s1,s2,s3)   % Image file: pX.jpg
    datafile=strcat(s11,s2); % Data   file: cedgeX
    cd('H:\Program\Sample image\In718 April06(2)');
    I=imread(name);
    cd('H:\Program');
    A=rgb2gray(I);
```

```
    corner1=[65,220];
    corner2=[1092,1020];
    xleft=corner1(1);
    yupp=corner1(2);
    xright=corner2(1);
    ydownp=corner2(2);
    A=A(yupp:ydownp,xleft:xright);
    B= im2double(A);
    [m,n]=size(B);
 % Find the characteristic intensity
    % Coil Region
     mark1=480;
     mark2=600;
     mark3=705;
     % Center Position determination
     [centerx,centery]=xycenter(B,mark1,mark3);
     % Edge intensity
     intensity=intens(B,centerx);
     recordl=0;
        % intensity=intensity-critical*(intensity-recordl);
        % critical value method
     intensity=0.6738;
     % edge detection region
[cyupc,cydownc,coillength,transion]=coil(B,centerx,mark1,mark2,mark3);
     % Set the start point
      if centery<=transion(1),
        ycenter=450;
        %ycenter=centery;
       else
        ycenter=centery;
    end
[ang11,r11]=radius11(B,centerx,centery,ycenter,intensity,transion(1),transion(2));
[ang22,r22]=radius22(B,centerx,centery,ycenter,intensity,transion(1),transion(2));
[ang33,r33]=radius33(B,centerx,centery,ycenter,intensity,transion(1),transion(2));
[ang44,r44]=radius44(B,centerx,centery,ycenter,intensity,transion(1),transion(2));
ang=[ang11,ang22,ang33,ang44];
    r=[r11,r22,r33,r44];
    cd('H:\Program\Data\Cedge');
    save(datafile,
'ang','r','ang11','ang22','ang33','ang44','r11','r22','r33','r44','centerx','centery',...
          'ycenter','intensity','coillength');
  clc;
 clear;
end
% Curve fitting
```

```
close all;
clc;
clear;
coil=189.5724;
cd('H:\Program\Data\Cedge\In713');
load cedgen30;
%Fitting and showing
cd('H:\Program');
[fity1,y1,reangright,p1]=right(r11,r44,ang11,ang44);
[fity2,y2,reangleft,p2]=left(r22,r33,ang22,ang33);
show(p1,p2);
hold on;
polar(ang,r,'x');
hold off;
% Radius Filter
[filterr1,filterang1,filterr4,filterang4]=filterright(r11,ang11,r44,ang44,fity1);
[filterr2,filterang2,filterr3,filterang3]=filterleft(r22,ang22,r33,ang33,fity2);
% Fitting and showing
[fityy1,yy1,reangrighty,p1y]=right(filterr1,filterr4,filterang1,filterang4);
[fityy2,yy2,reanglefty,p2y]=left(filterr2,filterr3,filterang2,filterang3);
figure;
show(p1y,p2y);
hold on;
angy=[filterang1,filterang2,filterang3,filterang4];
ry=[filterr1,filterr2,filterr3,filterr4];
polar(angy,ry,'x');
hold off;
% Compute
      mass=358.9;
      coill=0.1564;
      global p11;
      global p22;
      global pixvalue;
      p11=p1y;
      p22=p2y;
      pixvalue=coill/coil;
      y11=quadl('volume1',0,pi);
      v1=2*y11*pi/3;
      densityrr=mass/v1*0.001;%%% Right+Right
      y22=quadl('volume2',0,pi);
      v2=2*y22*pi/3;
      densityll=mass/v2*0.001;%%% Left+Left
      densityrl=2*mass/(v1+v2)*0.001;%%% Right+Left
      value1=[densityrr,densityll,densityrl,intensity];
```

APPENDIX B

THE SOURCE CODE FOR NUMERICAL MODEL OF MODULATED POWER METHOD

```
% Modulated heating method simulation
  clc;
 clear;
 load powerdata;
%-------Material Property ---------------------------------
   S_b=5.67*10^-8;
   K=76;
   Cp=620;
   Den=7905;
   Emis=0.22;
   ti=300;   % enviroment temp
   R_sample=2; % unit: mm
   ele_cond=5e6;
   permea_vacuum=4*pi*10^-7;
   skin=sqrt(2/(200e3*ele_cond*permea_vacuum);
   h=R_sample*sin(10*pi/180);
   h1=(R_sample-skin)*sin(10*pi/180);
   V_heat=2*pi*h^2*(R_sample-h/3)- 2*pi*h1^2*(R_sample-skin-h1/3);
   volume=4*pi*R_sample^3/3;
   mass=Den*volume*(1e-9);
   A=4*pi*R_sample^2*(1e-6);
% Discritize time and space domain
   dt=0.05;
   tfinal=2;
   Nr=20;
   Ntheta=30;
   dr=R_sample/(Nr);
   dtheta=pi/2/(Ntheta-1);
    Tmatrix=ones(Ntheta*Nr+1,1)*1915.1;
     Eqr=zeros(Nr*Ntheta+1,1);
     Eql=zeros(Nr*Ntheta+1,Nr*Ntheta+1);
     hp=0; % Power indicator
     for tt=dt:dt:tfinal,
          tt
          hp=hp+1;
       % Inside node
          for row=2:Ntheta-1,
               for colum=1:Nr-1,
                   node=colum+(row-1)*Nr;
                   theta=pi/2-dtheta*(row-1);
                   r=colum*dr ;
                   Ar=(r)^2*sin(theta)*dtheta*pi/2*(1e-6);
                   Ar1=(r-0.5*dr)^2*sin(theta)*dtheta*pi/2*(1e-6); %Inside(m^2)
Ar2=(r+0.5*dr)^2*sin(theta)*dtheta*pi/2*(1e-6); % Outside
Aa1=r*sin(theta-0.5*dtheta)*pi*dr/2*(1e-6);       % Up
```

```
Aa2=r*sin(theta+0.5*dtheta)*pi*dr/2*(1e-6);       % Down
                c1=Den*Cp*Ar*dr*(1e-3)/dt;
                c2=-K*Aa1/(r*(1e-3)*dtheta);
                c3=K*Aa2/(r*(1e-3)*dtheta);
                c4=-K*Ar1/(dr*(1e-3));
                c5=K*Ar2/(dr*(1e-3));
                      Eql(node,node-Nr)=-c3;
                      Eql(node,node)=c1-c2+c3-c4+c5;
                      Eql(node,node+1)=-c5;
                      Eql(node,node+Nr)=c2;
                    if (theta>80*pi/180) & (r>R_sample-skin),
                       Q=power(hp)/V_heat;
                    else
                       Q=0;
                    end;
                      Eqr(node)=c1*Tmatrix(node)+Q*Ar*dr;
    if row==2     % Because the center located node-1 position
                      Eql(node,end)=c4;
                    else
                      Eql(node,node-1)=c4;
                    end
            end
          end
    % Surface node
       colum=Nr;
        for row=2:Ntheta-1,
            node=colum+(row-1)*Nr;
            theta=pi/2-dtheta*(row-1);
            r=colum*dr;
            Aa1=r*sin(theta-0.5*dtheta)*pi*dr/2*(1e-6)/2;
            Aa2=r*sin(theta+0.5*dtheta)*pi*dr/2*(1e-6)/2;
            Ar=(r)^2*sin(theta)*dtheta*pi/2*(1e-6);
            Ar1=(r-0.5*dr)^2*sin(theta)*dtheta*pi/2*(1e-6);
ha=S_b*Emis*(Tmatrix(node)^2+ti^2)*(Tmatrix(node)+ti);
c1=Den*Cp*Ar*dr*(1e-3)/dt;
                c2=-K*Aa1/(r*(1e-3)*dtheta);
                c3=K*Aa2/(r*(1e-3)*dtheta);
                c4=-K*Ar1/(dr*(1e-3));
                c5=-ha*Ar;
                      Eql(node,node-Nr)=-c3;
                      Eql(node,node)=c1-c2+c3-c4-c5;
                      Eql(node,node+Nr)=c2;
                      Eql(node,node-1)=c4;
                   if (theta>80*pi/180) ,
                      Q=power(hp)/V_heat;
```

```
                    else
                        Q=0;
                    end;
                      Eqr(node)=c1*Tmatrix(node)-c5*ti+Q*Ar*dr;
end
      % Boundary nodes
        row=1;
            for colum=1:Nr,
              node=colum+(row-1)*Nr;
              Eql(node,node)=1;
              Eql(node,node+Nr)=-1;
            end
            row=Ntheta;
            for colum=1:Nr,
              node=colum+(row-1)*Nr;
              Eql(node,node)=1;
              Eql(node,node-Nr)=-1;
            end
         % Center
            Eql(Nr*Ntheta+1,Nr*Ntheta+1)=1;
            Eql(Nr*Ntheta+1,1)=-1;
          % Solve
          Tmatrix=inv(Eql)*Eqr;
          center(hp)=Tmatrix(1);
          side(hp)=Tmatrix(Nr);
        end
%function power=getpower(pos,I)
  f= 200000;
  sample_ID=1;
[permea_vacuum,s_b,permea,permea_,conduc,emmis,R_sample,Density]=getsample(sa
mple_ID);
    coil_ID=1;
    [n_upper,n_lower,span,d,R_coil]=getcoil(coil_ID);
    coillength=(n_lower-1)*d+(n_upper-1)*d+span;
    % Calculate the levitation force
            % Calculate Gx,Fx
              x=R_sample*sqrt(pi*conduc*f*permea_);
              xx=2*x;
              if (x>1000),
                  Gx=1.0;
                  Fx=x;
              else
               temp1=3*(sinh(xx)-sin(xx));
               temp2=4*x*(sinh(x)^2+sin(x)^2);
               Gx= 1-temp1/temp2;
```

```
Fx=(x*sinh(xx)+x*sin(xx)-cosh(xx)+cos(xx))/(cosh(xx)-cos(xx));
end;
  % Calculate the item1 ~ item4
          z=pos/1000;
       for n=1:1:n_lower,
            z_l(n)=-(span/2+(n-1)*d);
          end;
          z_l=rot90(z_l,2);
          for n=1:n_upper,
            z_u(n)=span/2+(n-1)*d;
          end;
          item1=0;
          item2=0;
          item3=0;
          item4=0;
          for n=1:n_lower,
            M=R_coil^2;
            temp1=(z-z_l(n))^2;
            temp2=(z-z_l(n));
            temp3(n)=M/((M+temp1)^1.5);
            temp4(n)=(M*temp2)/((M+temp1)^2.5);
          end;
          item3=sum(temp3);
          item4=sum(temp4);
          for n=1:n_upper,
            M=R_coil^2;
            temp1=(z-z_u(n))^2;
            temp2=(z-z_u(n));
            temp5(n)=M/((M+temp1)^1.5);
            temp6(n)=(M*temp2)/((M+temp1)^2.5);
          end;
          item1=sum(temp5);
          item2=sum(temp6);
         F_upper=9/8*permea_*I*I*Gx*item1*item2;
           F_upper=F_upper/9.8/1000;              % (g/cm^3)
         p_upper=3*pi*R_sample*(0.5*I*item1)^2*Fx/conduc;
         F_lower=9/8*permea_*I*I*Gx*item3*item4;
           F_lower=F_lower/9.8/1000;              % (g/cm^3)
         p_lower=3*pi*R_sample*(0.5*I*item3)^2*Fx/conduc;
         F=F_lower+F_upper;
         p=p_upper+p_lower;
      power=p;
function force=getforce(pos,I2)
  I=I2;
   f= 200000;
```

```
    % Analytical Model of EML
    % Load the thermophysical properties of the sample and sample size
     sample_ID=1;
[permea_vacuum,s_b,permea,permea_,conduc,emmis,R_sample,Density]=getsample(sa
mple_ID);
     coil_ID=1;
     [n_upper,n_lower,span,d,R_coil]=getcoil(coil_ID);
     coillength=(n_lower-1)*d+(n_upper-1)*d+span;
            x=R_sample*sqrt(pi*conduc*f*permea_);
             xx=2*x;
             if (x>1000),
                  Gx=1.0;
                  Fx=x;
             else
              temp1=3*(sinh(xx)-sin(xx));
              temp2=4*x*(sinh(x)^2+sin(x)^2);
              Gx= 1-temp1/temp2;
Fx=(x*sinh(xx)+x*sin(xx)-cosh(xx)+cos(xx))/(cosh(xx)-cos(xx));
             end;
             z=pos/1000;
        for n=1:1:n_lower,
                z_l(n)=-(span/2+(n-1)*d);
           end;
           z_l=rot90(z_l,2);
           for n=1:n_upper,
                z_u(n)=span/2+(n-1)*d;
           end;
           item1=0;
           item2=0;
           item3=0;
           item4=0;
           for n=1:n_lower,
                M=R_coil^2;
                temp1=(z-z_l(n))^2;
                temp2=(z-z_l(n));
                temp3(n)=M/((M+temp1)^1.5);
                temp4(n)=(M*temp2)/((M+temp1)^2.5);

           end;
           item3=sum(temp3);
           item4=sum(temp4);
           for n=1:n_upper,
                M=R_coil^2;
                temp1=(z-z_u(n))^2;
                temp2=(z-z_u(n));
```

```
            temp5(n)=M/((M+temp1)^1.5);
            temp6(n)=(M*temp2)/((M+temp1)^2.5);

        end;
        item1=sum(temp5);
        item2=sum(temp6);
       F_upper=9/8*permea_*I*I*Gx*item1*item2;
       F_upper=F_upper/9.8/1000;                % (g/cm^3)
       p_upper=3*pi*R_sample*(0.5*I*item1)^2*Fx/conduc;
       F_lower=9/8*permea_*I*I*Gx*item3*item4;
         F_lower=F_lower/9.8/1000;              % (g/cm^3)
       p_lower=3*pi*R_sample*(0.5*I*item3)^2*Fx/conduc;
       F=F_lower+F_upper;
       p=p_upper+p_lower;
    force=F;
function
[permea_vacuum,s_b,permea,permea_,conduc,emmis,R_sample,Density]=getsample(sa
mple_ID)
        permea_vacuum=4*pi*10^-7;
        s_b=5.67*10^-8;
        permea=1;
        permea_=permea*permea_vacuum;
        conduc=3.85e6;    % Iron Sample
        emmis=0.34;
        R_sample=0.002;
        Density=7.8;    %% g/cm^3
function k=stiffspring(I,bottom,top)
 f= 200000;
   % Analytical Model of EML
   % Load the thermophysical properties of the sample and sample size
    sample_ID=1;
[permea_vacuum,s_b,permea,permea_,conduc,emmis,R_sample,Density]=getsample(sa
mple_ID);
    coil_ID=1;
    [n_upper,n_lower,span,d,R_coil]=getcoil(coil_ID);
    coillength=(n_lower-1)*d+(n_upper-1)*d+span;
    % Calculate the levitation force
        % Calculate Gx,Fx
          x=R_sample*sqrt(pi*conduc*f*permea_);
          xx=2*x;
          if (x>1000),
               Gx=1.0;
               Fx=x;
          else
           temp1=3*(sinh(xx)-sin(xx));
```

```
                temp2=4*x*(sinh(x)^2+sin(x)^2);
                Gx= 1-temp1/temp2;
Fx=(x*sinh(xx)+x*sin(xx)-cosh(xx)+cos(xx))/(cosh(xx)-cos(xx));
              end;
           h=1;
           low_limit=bottom;
            up_limit=top;
         dz=coillength/500;
            for z=low_limit:dz:up_limit, %   Sample's position

             for n=1:1:n_lower,
                  z_l(n)=-(span/2+(n-1)*d);
             end;
             z_l=rot90(z_l,2);
             for n=1:n_upper,
                  z_u(n)=span/2+(n-1)*d;
             end;
             item1=0;
             item2=0;
             item3=0;
             item4=0;
             for n=1:n_lower,
                  M=R_coil^2;
                  temp1=(z-z_l(n))^2;
                  temp2=(z-z_l(n));
                  temp3(n)=M/((M+temp1)^1.5);
                  temp4(n)=(M*temp2)/((M+temp1)^2.5);
             end;
             item3=sum(temp3);
             item4=sum(temp4);
             for n=1:n_upper,
                  M=R_coil^2;
                  temp1=(z-z_u(n))^2;
                  temp2=(z-z_u(n));
                  temp5(n)=M/((M+temp1)^1.5);
                  temp6(n)=(M*temp2)/((M+temp1)^2.5);
             end;
             item1=sum(temp5);
             item2=sum(temp6);
               F_upper(h)=9/8*permea_*I*I*Gx*item1*item2;
              F_upper(h)=F_upper(h)/9.8/1000;
p_upper(h)=3*pi*R_sample*(0.5*I*item1)^2*Fx/conduc;
            F_lower(h)=9/8*permea_*I*I*Gx*item3*item4;
              F_lower(h)=F_lower(h)/9.8/1000;
p_lower(h)=3*pi*R_sample*(0.5*I*item3)^2*Fx/conduc;
```

```
    F(h)=F_lower(h)+F_upper(h);
    p(h)=p_upper(h)+p_lower(h);
    h=h+1;
end;
  Site=low_limit:dz:up_limit;
  volum=4*pi*(100*R_sample)^3/3;
  F=F*volum*9.8/1000;
  [k,s]=polyfit(Site,F,1);
  Ffit=polyval(k,Site);
  figure;
  plot(Site,F,Site,Ffit);
  legend('Levitation','Fitted');
  ylabel('Levitation force N');
  xlabel('Position (m)');
```

APPENDIX C

THE SOURCE CODE FOR ANALYSIS OF TEMPERATURE DATA

```
clc;
clear;
sample=50;%% Sampling rate
dataset=xlsread('Da');
dataset=dataset(1:2:end,:);
time=dataset(:,1);
temp=dataset(:,2);
power=dataset(:,3);
M=[time,temp,power];
%Fit time range
 time1=300;
 time2=410;
 data=cutime(time1,time2,time,temp,power);
 % Display
 time=data(:,1);
 temp=data(:,2);
 power=data(:,3);
 %
 subplot(2,1,1),
 plot(time,temp);
 xlabel('time(s)');
 ylabel('Temperature (C)');
 subplot(2,1,2);
 plot(time,power);
 ylabel('Control voltage(V)');
  %
 shift=mean(temp);
 temp1=temp-shift;
 [b,a] = butter(5,1/(sample/2));
 Hd = dfilt.df2t(b,a);
 fitemp= filter(Hd,temp1)+shift;
 %
 point=100;
 fitemp=fitemp(point:end);
 power=power(point:end);
 time=time(point:end)-time(point);
  figure;
 subplot(2,1,1);
 plot(time,fitemp);
 xlabel('time(s)');
 ylabel('Temperature (C)');
 subplot(2,1,2);
 plot(time,power);
 ylabel('Control voltage(V)');
 %xlswrite('Noisefree',[time,fitemp,power]);
```

```
% Data Analysis
 clc;
 clear;
 numerical= xlsread('Noisefree');
 time=numerical(:,1);
 temp=numerical(:,2);
 power=numerical(:,3);
 %% Display
 subplot(2,1,1);
 plot(time,temp);
 ylabel('Temperatur (C)');
 subplot(2,1,2);
 plot(time,power);
 xlabel('time(s)');
 ylabel('Control voltage(V)');
 % curve fitting
   % DC
   time1=160;
   time2=180;
   temp_dc=findmean(time,temp,time1,time2);
   %% Amplitude
   %% Phase angle
   time1=160;
   time2=180;
   f=0.15;
   [ampli,dc,phase]=sinfit(time,temp,time1,time2,f);
function [ampli,dc,phase]=sinfit(time,temp,time1,time2,f)
 % Trim data
  index1=find(time>=time1);
  index1=index1(1);
  index2=find(time>=time2);
  index2=index2(1);
  temp=temp(index1:index2);
  time=time(index1:index2);
   dcini=(max(temp)+min(temp))*0.5;
   acini=(max(temp)-min(temp))*0.5;
   % Phase
   w=2*pi*f;
   h=0;
    for theta=0:pi/180:2*pi,
        fitemp=dcini+acini*sin(w*time+theta);
        h=h+1;
        subtr=abs(fitemp-temp);
        residual(h)=sum(subtr);
        thetar(h)=theta;
```

```
 end
 [record,index]=min(residual);
 phase=thetar(index);
    for dc=dcini-2:0.1:dcini+2,
        for ampli=acini-1:0.1:acini+1,
        fitemp=dc+ampli*sin(w*time+phase);
         h=h+1;
        subtr=abs(fitemp-temp);
        residual(h)=sum(subtr);
        dcr(h)=dc;
        amplir(h)=ampli;
        end
  end
    [record,index]=min(residual);
    dc=dcr(index);
    ampli=amplir(index);
% Display
 fitemp=dc+ampli*sin(w*time+phase);
 plot(time,temp,time,fitemp,'--');
 xlabel('time(s)');
 ylabel('Temperatur (C)');
 legend('Original data','fitted data');
```